VOLUME 32 JULY 1954 NUMBER 7

Canadian Journal of Physics

Published by THE NATIONAL RESEARCH COUNCIL
OTTAWA CANADA

CANADIAN JOURNAL OF PHYSICS

(*Formerly Section A, Canadian Journal of Research*)

Under the authority of the Chairman of the Committee of the Privy Council on Scientific and Industrial Research, the National Research Council issues annually THE CANADIAN JOURNAL OF PHYSICS and six other journals devoted to the publication of the results of original scientific research. Matters of general policy concerning these journals are the responsibility of a joint Editorial Board consisting of: members representing the National Research Council of Canada; the Editors of the Journals; and members representing the Royal Society of Canada and four other scientific societies.

Manuscripts for publication should be submitted to Dr. Léo Marion, Editor-in-Chief, Canadian Journal of Physics, National Research Council, Ottawa 2, Canada.
(For instructions on preparation of copy, see **Notes to Contributors** (inside back cover).)

Proof, correspondence concerning proof, and *orders for reprints* should be sent to the Manager, Editorial Office (Research Journals), Division of Administration, National Research Council, Ottawa 2, Canada.

Subscriptions, renewals, and orders for single or back numbers should be sent to Division of Administration, National Research Council, Ottawa 2, Canada. Remittances should be made payable to the Receiver General of Canada, credit National Research Council.

The journals published, frequency of publication, and prices are:

Canadian Journal of Biochemistry and Physiology	Bimonthly	$3.00 a year
Canadian Journal of Botany	Bimonthly	$4.00 a year
Canadian Journal of Chemistry	Monthly	$5.00 a year
Canadian Journal of Microbiology*	Bimonthly	$3.00 a year
Canadian Journal of Physics	Monthly	$4.00 a year
Canadian Journal of Technology	Bimonthly	$3.00 a year
Canadian Journal of Zoology	Bimonthly	$3.00 a year

The price of single numbers of all journals is 75 cents.

*Volume 1 will combine three numbers published in 1954 with six published in 1955 and will be available at the regular annual subscription rate of $3.00.

Canadian Journal of Physics

Issued by THE NATIONAL RESEARCH COUNCIL OF CANADA

VOLUME 32 JULY 1954 NUMBER 7

ON THE ANALYSIS OF EXPERIMENTS INVOLVING THE KINETICS OF PILES WITH REFLECTORS[1]

BY V. H. RUMSEY[2]

ABSTRACT

The theory of pile kinetics is used to analyze measurements of the mean lifetime and migration length of neutrons. The purpose is to show what effects need to be taken into account in the analysis of pile experiments rather than to give a precise experimental verification of the theory. It is shown that the bare-pile one-group model is not adequate. A two-group model which takes into account the presence of the reflector is used to obtain a more accurate analysis. The orders of magnitude are illustrated by deriving formulas for a specific pile—the Chalk River ZEEP. It is found that the presence of the reflector results in an increase of the mean lifetime T of about 20%. Increasing the multiplication constant k_∞ by a given amount produces a bigger value of effective multiplication constant k_e for the pile with a reflector than without, but owing to the larger value of T, the pile with reflector diverges more slowly than the bare pile. The bare-pile model overestimates by about 10% the change in k_∞ required to re-establish stability after a given change in k_e. The migration length is overestimated by about 25%. The more elaborate theory agrees well with various measured values, but this is partly fortuitous because the structure of the ZEEP is rather complex and is not adequately represented in the theory.

INTRODUCTION

Various experiments on the ZEEP have shown that the simple one-group model based on the assumption of a bare pile (3, 4) for the analysis of pile kinetics is not consistent with the actual behavior of ZEEP. This is not surprising because the one-group model applies strictly to a bare pile for which the reproduction constant is very slightly greater than unity. The experiments of Fergusson and Gilbert (2) bring out one aspect of the matter. These investigators measured the effect on the pile power of an absorber whose rate of absorption was made to oscillate sinusoidally with periods from 0.5 to 500 sec. They found that the mean lifetime of a neutron as derived from their results was significantly greater than the value calculated from cross sections, etc. on the basis of the bare-pile model. The experiments of Bayly (1) bring out another aspect. Here, the time variation of pile power was measured after the depth of heavy water, denoted by h, had been changed by a known amount from the value which gave steady power. He found that the migration length of neutrons derived from the experiment is significantly greater than the value obtained by other means, again assuming that a bare-pile model is applicable.

[1] *Manuscript received January 25, 1954.*
Contribution from Atomic Energy of Canada Limited, Chalk River, Ont. Issued as A.E.C.L. No. 105.

[2] *Present address: Ohio State University, Columbus, Ohio.*

Our aim is, then, to analyze experiments of the following type. Suppose that the pile is running at a steady power and that h is suddenly increased by an amount δh. As a result the pile power will start to rise. We wish to determine the relation between the way in which the power changes with the time and δh.

In order to give point to the method described here, we will review the procedure which has been adopted in such cases. It is argued that increasing h by δh above the critical height is equivalent to increasing k_∞, the multiplication constant defined with respect to a lattice extending to infinity. The increase in k_∞ is calculated from a formula of the form

$$[1] \qquad k_\infty - 1 = \kappa^2 M^2$$

or some more refined form where κ^2 represents the Laplacian, which is determined from h and M, the migration length of the fissile medium. It is assumed that the amount by which k_∞ would have to be reduced in order to re-establish steady power is equal to the value of $k_e - 1$, where k_e represents the effective multiplication constant at height δh above critical height. This is one assumption that introduces some error. Again it is assumed that the mean lifetime τ which goes with k_e is equal to the mean lifetime of a neutron in the infinite medium, that is, the average time between the birth and death of a neutron if it spent all of its life in the heavy water – uranium lattice. This procedure is accurate for an infinite pile but only approximately valid for piles of finite size. For instance, it does not take into account the fact that the average lifetime of a neutron is somewhat lengthened because a significant number of neutrons pass through the reflector before being finally captured in the lattice, and, owing to the small capture cross section of the reflector, a neutron can spend a relatively long time over this process.

METHOD OF ANALYSIS

The difficulty with the application of the simple theory appears to be mainly due to the fact that quantities like k_e and τ are not clearly defined for a pile such as the ZEEP, which is neither "bare" nor infinite: it consists of a tank containing the heavy water – uranium lattice and a graphite reflector. It can be shown (6), on the basis of a two-group model, that the simple equations can still be retained for such cases, provided we define the effective multiplication constant and mean lifetime as follows.

The mean lifetime to be used is the average time between the birth and death of a neutron in the tank. This average time will be an average over all possible ways in which a neutron starting out from fission somewhere in the tank finally gets captured as a thermal neutron in the tank, and obviously is influenced by the presence of the reflector. To give some idea of the orders of magnitude involved, we note that the mean lifetime of a neutron which spends all of its life in the tank is about 0.7 msec., whereas the mean lifetime of a neutron which spends all of its life in the reflector is about 14 msec., and the actual mean lifetime, T, which we have defined above is some average between these two values.

Let us denote the lifetime of a neutron which spends all of its life in one

medium by the Greek letter τ. Thus τ is a property of the medium; in the case of monokinetic neutrons it is the capture mean free path divided by the neutron velocity.

The effective multiplication constant k_e which has to be used in conjunction with the mean lifetime T is defined as k_∞ times the probability that a neutron that is born in the tank will die in the tank. Since this probability is found by taking the average over all possible ways in which the process takes place, k_e also depends upon the presence of the reflector. Note that neither T nor k_e is dependent in any way on the fact that there may be delayed neutron sources or γ–n sources as well as the ordinary prompt fission sources. We can make use of this in order to simplify the derivation of a formula relating $k_e - 1$ and the amount by which k_∞ would have to be changed in order to re-establish stability. We consider a pile which is identical to the actual pile in all respects, except that all neutron sources in it are prompt sources; in particular, the distribution of neutron sources is the same in the actual and "prompt" piles. It follows that k_e and T are the same in these two piles.

In order to illustrate the method we adopt a very simple model. Suppose that the pile is spherically symmetrical, that the diffusion coefficients are equal in the tank and reflector, and that a one-group approximation is valid. To be specific, assume that $k_e > 1$. Then the prompt pile diverges like $\exp \omega t$ where

[2] $$\omega T = k_e - 1.$$

This follows immediately from the definitions of k_e and T. Now whether or not the pile is diverging, the neutron density is a solution of equations like

[3] $$\begin{aligned} (\nabla^2 + \alpha^2)\rho &= 0 \qquad \text{in the tank,} \\ (\nabla^2 - \lambda^2)\rho &= 0 \qquad \text{in the reflector,} \end{aligned}$$

and the critical condition which always has to be satisfied is

[4] $$\alpha \cot \alpha a + \lambda = 0$$

where "a" is the radius of the tank. If by some means α and λ are varied, but "a" remains constant, then

[5] $$\delta\alpha \left[\frac{\lambda}{\alpha} + \left(1 + \frac{\lambda^2}{\alpha^2}\right) a\alpha \right] = \delta\lambda.$$

We now consider two cases—(1) the diverging prompt pile, and (2) the same pile in which we have reduced k_∞ to say k'_∞ in order to re-establish stability. We take for the values of $\delta\alpha$ and $\delta\lambda$ in [5] the difference between the values of α and λ in the first and second cases. For the diverging pile it is readily verified that

[6] $$M^2\alpha^2 = k_\infty - 1 - \omega\tau_c$$

where τ_c is equal to the value of τ in the tank, and M is the migration length in the tank, and

[7] $$L_r^2 \lambda^2 = \omega\tau_r + 1$$

where τ_r is equal to the value of τ for the reflector and L_r is the migration length in the reflector. For the static pile we have

[8] $$M^2 \alpha'^2 = k'_\infty - 1$$

and

[9] $$L_r^2 \lambda'^2 = 1.$$

From [8] and [6] we obtain

[10] $$M^2 2\alpha \, \delta\alpha = k_\infty - k'_\infty - \omega\tau_c,$$

and from [7] and [9] we obtain

[11] $$L_r^2 2\lambda \, \delta\lambda = \omega\tau_r.$$

Note that the assumption of equal diffusion coefficients in the tank and reflector implies

[12] $$M^2 \tau_r = L_r^2 \tau_c.$$

Substitution from [2], [10], and [11] in [5] gives the following relation between $k_e - 1$ and $k_\infty - k'_\infty$:

[13] $$(k_\infty - k'_\infty)T = (k_e - 1)\tau_c \left[1 + \left\{ \frac{1}{\kappa^2 L_r^2} + \frac{a}{L_r} \left(1 + \frac{1}{\kappa^2 L_r^2} \right) \right\}^{-1} \right]$$

in which we have denoted the steady state value of α by κ in order to conform to the usual notation.

It will be noted that contrary to the usual assumption, $k_e - 1$ and $k_\infty - k'_\infty$ are not equal but differ by an amount which diminishes as the size of the pile increases.

It need hardly be added that the change of k_∞ required for the prompt pile is identical to that required for the actual pile since k_∞ does not depend on delayed neutrons, etc.

We can now determine the value of $k_e - 1$ due to raising h above the critical value by an amount δh, by finding the amount by which we would have to reduce k_∞ in order to have a stable pile at height $h + \delta h$. The actual evaluation of this relation is given below, where we consider the specific case of the ZEEP. The formula [13] is not valid in the ZEEP because the simplifying assumptions we made in order to derive it do not hold.

The method of evaluating the mean lifetime T can be illustrated by means of the following simple model. Suppose that all neutrons in the system have the same velocity. Of the total assembly of neutrons in the whole system (tank and reflector) let N be the number in the tank and n the number destined to die in the tank. (Note the difference—many neutrons in the reflector may be destined to die in the tank.) Then

[14] $$N = \int \rho \, dv$$

where ρ is given by equations [3] and the integral is taken over the volume of the tank. To find the value of n, i.e. the number of neutrons destined to die in the tank, we regard the actual neutron distribution as a distribution of sources, and solve for the new distribution which would arise from this distribution of sources. In other words, n is given by

[15] $$n = \int X \, dv$$

taken over the volume of the tank, where

$$[16] \qquad \begin{aligned} X - M^2 \nabla^2 X &= \rho\tau_c \text{ in the tank,} \\ X - L^2 \nabla^2 X &= \rho\tau_r \text{ in the reflector.} \end{aligned}$$

Equations [16] imply that if $\int \rho \, dv$ is the actual number of neutrons in a given volume, then $\int (X/\tau) \, dv$ is the number that are destined to die in that volume.

Now we can express T in terms of these quantities by noting that the rate at which neutrons are dying in the tank can be represented as either N/τ or n/T. Equating these two expressions and substituting for N and n from [14] and [15] we obtain the following formula for T:

$$[17] \qquad T = \int X \, dv / \int \rho \, dv,$$

the integrals being taken over the volume of the tank.

The mean lifetime T is a fundamental constant of the system. It can be measured by using the delayed neutron periods as a time standard. In the experiments of Gilbert and Fergusson, to which we have referred, measurement of the phase difference between the k_e and power oscillations as a function of frequency is an elegant way of determining T.

The quantity $k_e - 1$ can be measured by analyzing the variation of pile power with time. By this means the value of $k_e - 1$ is obtained relative to c, where c is that fraction of the total yield of neutrons from fission that are delayed.

THE VALIDITY OF THE ONE- AND TWO-GROUP REPRESENTATIONS

The one- and two-group models are usually compared with reference to a static system. On this basis the simple one-group model works quite well for, say, the ZEEP. However the approximations involved in a time dependent problem are not of the same kind as in a static problem. For instance the static solution depends on the slowing down length, L_f, and thermal migration length, L, about equally, because in most cases L_f and L are approximately equal. In a time dependent case the times taken for slowing down and thermal migration are important and since the slowing down time is much smaller, the thermal migration is relatively much more important in the time dependent problem than in the static problem.

The different nature of the approximations involved in the static and kinetic problems is brought out even in the simple case of a bare pile. The values obtained for T on the basis of one- and two-group models in this case are significantly different. We obtain:

$$\text{one-group } T = \tau_c / k_\infty,$$

$$\text{two-group } T = \tau_t / (1 + \kappa^2 L^2) + p\tau_f / (1 + \kappa^2 L_f^2)$$

where p = probability of escaping resonance capture in uranium,

and $\tau_c = \tau_t + \tau_f$

is the one-group τ, the sum of "fast" and thermal τ's, and L_f and L are the slowing down and thermal diffusion lengths. Putting $L^2 = L_f^2$ and using the approximate relation

$$(L^2 + L_f^2)\kappa^2 = k_\infty - 1$$

we have

$$\text{one-group } T = (\tau_f + \tau_t)/k_\infty,$$
$$\text{two-group } T = (p\tau_f + \tau_t)/[1 + \tfrac{1}{2}(k_\infty - 1)].$$

If $k_\infty = 1.2$, as in the ZEEP, there is a 10% difference, but what is more important from our point of view is that the correction due to the pile not being infinite (in which case T would be $\tau_f + \tau_t$) differs by a factor of two between the two models. Thus it is clear that the one-group model is inadequate for the purpose of calculating T. On the other hand the formula relating $k_e - 1$ and the change of k_∞ has the same form for a bare pile however many groups we use, i.e.

$$k_\infty(k_e - 1) = k_\infty - k'_\infty.$$

APPROXIMATIONS USED IN THE FORMULA FOR T

In order to reduce the algebra while retaining a sufficiently accurate representation, we adopt the following device for the calculation of T. We note that the time spent in slowing down in either the tank or the reflector is less, by an order of magnitude, than the time during which a neutron migrates with thermal velocities. Furthermore, the slowing down times in tank and reflector are more nearly equal than the thermal lifetimes. We can therefore put

$$T \doteq \tau_f + T_t$$

where τ_f is the value of τ corresponding to slowing down in the tank and T_t the average time between birth of a thermal neutron in the system (tank and reflector) and its death in the tank. Thus T_t is calculated by means of the formula [17], i.e.

$$T_t = \int X\, dv / \int \rho_t\, dv$$

where

[18] $$X = L^2 \nabla^2 X + \tau_t \rho_t \text{ in the tank,}$$

[19] $$X = L_r^2 \nabla^2 X + \tau_{tr} \rho_t \text{ in the reflector.}$$

In these equations ρ_t is the density of thermal neutrons.

To determine T we therefore have to find a sufficiently accurate representation of the thermal neutron distribution in the system. As is well known, the one-group model gives a good representation of ρ_t in the tank except at points within a migration length of the tank wall; in the reflector the form of ρ_t is again in agreement with measurement except at points near the tank. However it can be shown that the one-group model underestimates the number of thermal neutrons in the reflector relative to the number in the tank, by a factor, say Q, which is about equal to two, as compared with a two-group model or models of more than two groups. In order to evade the turgid algebra associated with the two-group calculation, we therefore take τ_t as being given by the one-group density in the tank and Q times the one-group density in the reflector. This then gives a sufficiently accurate representation of the relative

numbers in tank and reflector and also of the spatial distribution in tank and reflector except for a small region near the tank wall.

The factor Q depends on the relaxation lengths in tank and reflector. If k_∞ is not much greater than unity Q is practically independent of the shape of the boundary between tank and reflector, and can therefore be evaluated by solving for the simplest possible geometry, e.g. for plane slabs or spheres. Assuming equal diffusion coefficients in tank and reflector the two-group model gives a value for Q which can be simplified to the following approximate form:

[20] $$Q \simeq (k_\infty - 1)/\kappa^2 L^2$$

which is accurate to within a few per cent if $k_\infty = 1.2$; L is the thermal diffusion length in the tank.

APPROXIMATIONS USED IN DERIVING A FORMULA FOR $k_e - 1$

To calculate the formula relating $k_e - 1$ and the equivalent change of k_∞ the two-group critical condition should be used in place of equation [4] but this is impracticable. Since the critical condition depends more on over-all effects rather than on individual neutron groups, the one-group model is satisfactory for this part of the calculation. Note that even if we modify the one-group model by means of the Q factor introduced above, the critical condition remains unchanged. This procedure does not imply that $k_e - 1$ is insensitive to the way in which the "fast" and thermal neutrons are distributed, but rather that a one-group model is good enough for the purpose of establishing the critical condition, especially since we shall fit it to the given pile geometry.

The next step in deriving the formula for $k_e - 1$ is to substitute values for $\delta\alpha$ and $\delta\lambda$ in the differential relation obtained from the critical condition, cf. equation [8]. As equations [6] and [7] show, $\delta\alpha$ and $\delta\lambda$ depend on time constants, e.g. $\omega\tau_c$ in [6], and consequently we must be cautious about using the one-group model here, because of the inaccuracies mentioned earlier. Actually it is not difficult to evaluate $\delta\alpha$ and $\delta\lambda$ by means of the two-group model. Adopting our previous notation in which unprimed quantities refer to the diverging prompt pile and primed quantities to the prompt pile in which we have reduced k_∞ to k'_∞ in order to make it static, in place of equation [6] the two-group model gives

$$(\alpha^2 L_f^2 + 1 + \omega\tau_f)(\alpha^2 L_t^2 + 1 + \omega\tau_t) = k_\infty$$

and in place of equation [8],

$$(\alpha'^2 L_f^2 + 1)(\alpha'^2 L_t^2 + 1) = k'_\infty$$

where

L_f and L_t are the fast and thermal diffusion lengths in the tank,

$$M^2 = L_t^2 + L_f^2,$$

τ_f and τ_t the fast and thermal values of τ in the tank,

and $$\tau_c = \tau_f + \tau_t.$$

Equation [10] is then replaced by

[21] $$2\alpha\,\delta\alpha(M^2 + 2\alpha^2 L_f^2 L_t^2) + \omega[\tau_c + \alpha^2(L_f^2\tau_t + L_t^2\tau_f)] = k_\infty - k'_\infty.$$

The two-group model gives the same relation as [11] for $\delta\lambda$ but with a slightly different interpretation:

$$2\lambda\,\delta\lambda = \omega\tau_1/L_1^2 \qquad [22]$$

where L_1 is the thermal diffusion length and τ_1 the thermal τ in the reflector.

To determine $k_e - 1$ our procedure is then to use the one-group critical condition but to interpret the parameters α and λ therein according to the two-group model.

CALCULATION OF T FOR THE ZEEP

The ZEEP is described in Reference (4). The ZEEP tank is cylindrical. We assume that the reflector is infinite and covers the curved sides only of the cylinder. Actually there is some reflector at the bottom of the ZEEP tank, but this is taken into account to some extent by fitting the constants to give the measured values of neutron distribution.

The details of the calculation are given in the Appendix. We obtain the following formula for T assuming equal thermal diffusion coefficients in tank and reflector:

$$T = \tau_f + \tau_t\left[\frac{1}{1+\kappa^2L^2} + \frac{Qa\beta^2}{2pqL^2}\,\frac{1-(K_0/K_1)^2}{(pI_0/I_1)+(qK_0/K_1)}\right] \qquad [23]$$

where

τ_f and τ_t are the fast and thermal values of τ in the tank,

κ^2 = Laplacian,

L = thermal diffusion length in the tank,

L_1 = thermal diffusion length in the reflector,

Q = the factor defined above in equation [20],

a = tank radius,

H = effective tank height,

$\beta^2 = \kappa^2 - (\pi/H)^2$,

$p^2 = (\pi/H)^2 + (1/L_1^2)$, (not to be confused with the resonance escape factor p),

$q^2 = (\pi/H)^2 + (1/L^2)$,

K_0 and K_1 are Bessel functions of imaginary argument ipa, and

I_0 and I_1 are Bessel functions of imaginary argument iqa.

It must be emphasized that this formula should be used only for assessing orders of magnitude; any agreement with experimental results will be a coincidence. This is partly due to the fact that we have not represented the ZEEP properly—the heavy water reflector at the bottom of the tank has not been allowed for at all well—and partly due to inadequate information about the "pile constants". The constants are assumed to have the following values:

κ^2 = 7.9 inverse meters^2 (measured value—Johns and Sargent (5)),

a = 1 meter,

H = 1.5 meters,

thermal diffusion length in reflector = 0.5 meters (measured value),

$L^2 = 125$ cm.^{2}—this is based on the assumption that $k_\infty = 1.2$ (by lattice calculation) and that

$L_f^2 = 115$ cm.^{2} The slowing down length, L_f^2, in the lattice is tied to a measured value to the indium resonance of 110 cm.^{2} for pure heavy water and cannot be far out. L^2 is then fixed through the measured Laplacian.

The controlling factors τ_f and τ_t cannot be estimated at all accurately. We have taken

$$\tau_f = \frac{3L_f^2}{l_t\,(\text{fast})}\,\frac{1}{9.1v}$$

where l_t is the transport mean free path and v the velocity of thermal neutrons (3).

Taking $v = 2.2 \times 10^3$ meters/sec.,

$l_t\,(\text{fast}) = 3.6$ cm.

gives $\tau_f = 0.05$ msec.

We assume that $$\tau_t = \frac{3L^2}{l_t(\text{thermal})\,v},$$

$l_t\,(\text{thermal}) = 2.4$ cm.

giving

$$\tau_t = 0.71 \text{ msec.}$$

Our formula then becomes

$$T = \tau_f + \tau_t\,(0.915 + 0.194).$$

The first two terms are what the value of T would be if there were no reflector. We see that the reflector constitutes a correction of the order of 20%. If we use the above values for τ_f and τ_t then

$$T = 0.84 \text{ msec.},$$

which happens to agree fairly well with the value of 0.86 msec. obtained by Fergusson and Gilbert (2).

CALCULATION OF THE VALUE OF $k_e - 1$ AND ASSOCIATED CALCULATION OF M^2

The assumptions listed above give the following formula for $k_e - 1$ (see Appendix):

[24] $$\frac{k_\infty - k'_\infty}{\tau_c} = \frac{k_e - 1}{T}\left[1 + \kappa^2 L_f^2 + \frac{M^2}{L^2}\,\frac{(K_1/K_0)^2 - 1}{(J_1/J_0)^2 + 1}\right]$$

in which the K and J Bessel functions have arguments pa and βa respectively. Substitution of the numerical values gives

$$\frac{k_\infty - k'_\infty}{\tau_c} = \frac{k_e - 1}{T}\,[1 + 0.09 + 0.144].$$

The expression on the left is what the time constant of the prompt pile would be if the pile were infinite, the expression on the right outside of the brackets

is the actual time constant of the prompt pile. The second term in brackets is due to the finite pile size and the third is due to the reflector. Substitution of the calculated values of T and τ_c gives

$$k_e - 1 = (k_\infty - k'_\infty)/1.1.$$

It is interesting to compare this with what the result would be if the ZEEP had no reflector. In this case

$$k_e - 1 = (k_\infty - k'_\infty)/k_\infty = (k_\infty - k'_\infty)/1.2.$$

Increasing k_∞ by a given amount thus produces a bigger value of $k_e - 1$ for the pile with a reflector than without, but owing to the much larger value of T in the former case, the pile with reflector diverges more slowly than the bare pile. It is worth noting that if we are given $k_e - 1$, then the bare-pile model overestimates $k_\infty - k'_\infty$ by about 10%.

The relation between $k_\infty - k'_\infty$ and δh, the increase of height over the critical value, needs careful examination for the ZEEP. For this purpose it seems desirable to make specific allowance for the heavy water reflector at the bottom of the tank. We consider the theoretical aspect in order to bring out the relevant details but here again theory cannot make a very accurate prediction. It does however suggest a way in which the desired relation can be obtained experimentally.

We have to find an expression for $\kappa^2 - \kappa'^2$ where κ^2 and κ'^2 are the Laplacians of the same pile, which in the unprimed case is the actual ZEEP and in the primed case is what the ZEEP would be if we reduced its k_∞ to k'_∞ in order to make it stable at the increased value of h.

In the cylindrical case, the radial and axial curvatures of the density are specified by β^2 and m^2 (see Appendix) where $\kappa^2 = \beta^2 + m^2$. We assume that the radial conditions are the same at any value of h. (There is an insignificant error in this assumption which is due to the fact that the height of the reflector is not kept in line with the height of core.) It follows that

$$\beta = \beta'.$$

Therefore

$$\kappa^2 - \kappa'^2 = m^2 - m'^2.$$

To illustrate the point suppose that the reflector at the bottom of the tank is of uniform thickness "t", and is characterized by a thermal diffusion length L. Let distance z be measured parallel to the pile axis from the bottom of the uranium rods, i.e. the reflector at the bottom of the tank extends from $z = 0$ to $z = -t$ and the lattice from $z = 0$ to $z = h$.

Adopting a one-group model, the density has the form

$$\sin m(h - z) \text{ in the lattice,}$$
$$\sinh (t + z)/L \text{ in the reflector.}$$

Since the diffusion coefficients are equal on either side, the boundary condition at $z = 0$ has the form

$$\tan mh + mL \tanh(t/L) = 0.$$

If the height is changed we see that

[25]

$$-(1/m) \tan mh = \text{constant} = \Lambda$$

where Λ is the ratio of ρ to $d\rho/dz$ at the plane through the bottom of the uranium rods and is a quantity that can be determined experimentally.

The change of m due to changing h by δh is thus given by

$$\delta m \left[h + \frac{\Lambda}{1 + \Lambda^2 m^2} \right] + \delta h\, m = 0. \tag{26}$$

The effective height H is given by

$$Hm = \pi \tag{27}$$

and is found by analysis of the vertical neutron distribution. If we put $\Lambda = 0$, we obtain the condition when there is no reflector below the rods. In this case $h = H$ and

$$\delta m\, H + \delta h\, m = 0. \tag{28}$$

Taking the following values

$H = 150$ cm.—effective height,

$h = 120$ cm.—height above bottom of rods,

we obtain from [25] and [27]

$$\Lambda = 35 \text{ cm.}$$

and equation [26] has the form

$$\delta m\ 143 + \delta h\, m = 0$$

to be compared with the relation [28] obtained by ignoring the reflector:

$$\delta m\ 150 + \delta h\, m = 0.$$

Ignoring the reflector therefore predicts a value for δm or $\kappa^2 - \kappa'^2$ due to a given δh that is about 5% too small.

If we take κ^2 as given by the two-group model, i.e.

$$(\kappa^2 L^2 + 1)(\kappa^2 L_s^2 + 1) = k_\infty,$$

then

$$(\kappa^2 - \kappa'^2)(2\kappa^2 L^2 L_s^2 + M^2) = k_\infty - k'_\infty. \tag{29}$$

Note that this differs from the one-group assumption

$$(\kappa^2 - \kappa'^2) M^2 = k_\infty - k'_\infty$$

by about 10%; the one-group model predicts, from given $\kappa^2 - \kappa'^2$ and $k_\infty - k'_\infty$, a value of M^2 that is too large by about 10%.

Summarizing the steps involved in finding the relation between $k_e - 1$ and h we have:

(*a*) Connection between $k_e - 1$ and $k_\infty - k'_\infty$,

(*b*) Connection between $k_\infty - k'_\infty$ and $\kappa^2 - \kappa'^2$,

(*c*) Connection between $\kappa^2 - \kappa'^2$ and δh,

and at each of these steps there is a difference from the conventional approximations of the order of 10%.

In terms of our equations the steps are:

$$[24] \quad (a) \quad k_e - 1 = -\delta k_\infty \frac{T}{\tau_c}\left[1 + \kappa^2 L_f^2 + \frac{M^2}{L^2}\frac{(K_1/K_0)^2 - 1}{(J_1/J_0)^2 + 1}\right]^{-1},$$

$$[29] \quad (b) \quad \delta k_\infty = \delta\kappa^2 \,(M^2 + 2\kappa^2 L^2 L_s^2),$$

$$[26] \quad (c) \quad \delta\kappa^2 = \delta m^2 = 2m\,\delta m = \frac{-2m^2\,\delta h}{h + \Lambda/(1 + \Lambda^2 m^2)}$$

from which we obtain the following formula for M^2:

$$[30] \quad M^2 + 2\kappa^2 L^2 L_s^2 = \frac{k_e - 1}{\delta h}\frac{\tau_c}{T}\left[1 + \kappa^2 L_f^2 + \frac{M^2}{L^2}\frac{(K_1/K_0)^2 - 1}{(J_1/J_0)^2 + 1}\right] \times \frac{1}{2m^2}\left[h + \frac{\Lambda}{1 + \Lambda^2 m^2}\right].$$

To illustrate the orders of magnitude suppose that $k_e - 1$ and δh are known, then the results obtained from the approximations listed below are:

(i) *Bare Pile—one-group model*

at step (*a*)	M^2 overestimated by about 10%
at step (*b*)	M^2 overestimated by about 10%
at step (*c*)	M^2 overestimated by about 5%
Total	M^2 overestimated by about 25%

(ii) *Bare Pile—two-group model*

at step (*a*)	M^2 overestimated by about 10%
at step (*b*)	no significant error
at step (*c*)	M^2 overestimated by about 5%
Total	M^2 overestimated by about 15%

(iii) *Bare Pile—age velocity model*

This differs from (ii) by one or two per cent.

The tendency is for the estimate of M^2 to come down as better models are used, cf. drop from 25% to 15% between (i) and (ii). The age velocity model applied to a bare pile overestimates M^2 by about 10%.

Substitution of the numerical values which we have assumed gives

$$M^2 + 2\,\kappa^2 L^2 L_s^2 = 1.03\,\frac{k_e - 1}{\delta h}\,\frac{H^3}{2\pi^2}.$$

If we had ignored the presence of the reflectors we would have obtained the erroneous result

$$M^2 + 2\,\kappa^2 L^2 L_s^2 = 1.18\,\frac{k_e - 1}{\delta h}\,\frac{H^3}{2\pi^2}.$$

Formula [30] is derived from a two-group model. A slight improvement in accuracy can be obtained by replacing $M^2 + 2\kappa^2 L^2 L_s^2$ by the expression for $\delta k_\infty/\delta\kappa^2$ obtained from the age velocity model.

APPENDIX

The solution of equations [3] written in terms of Bessel functions is

[100] $\rho_0 = A \cos mz\, J_0(\beta r)$ in the tank,

[101] $m = \pi/H, \quad \beta^2 = \kappa^2 - m^2,$

[102] $\rho_1 = B \cos mz\, K_0(pr)$ in the reflector,

[103] $p^2 = (1/L_1^2) + m^2,$

r = distance from axis,

z = distance along axis,

which satisfy the boundary conditions at $z = \pm\frac{1}{2}H$, $r = 0$ and at $r = \infty$.

Assuming equal diffusion coefficients in tank and reflector and equating densities and currents at the tank wall $r = a$ we have

[104] $AJ_0(\beta a) = BK_0(pa),$

[105] $AJ_1(\beta a) = pBK_1(pa),$

giving the critical condition

[106] $pJ_0(\beta a)\, K_1(pa) = J_1(\beta a)\, K_0(pa).$

Formula for T

As explained in the text the density of thermal neutrons is represented by ρ_0 (equation 100) in the tank and $Q\rho_1$ (equation 102) in the reflector. Evidently the dependence on z is the same for all densities so that it can be omitted in what follows. The solutions involve three kinds of Bessel functions and since these are defined differently in different books, it is perhaps worth stating the properties by which we define them here. Denoting differentiation with respect to the argument by a dash, (assuming real arguments):

$J'_0 = -J_1$, J_0 always finite, zero at ∞;

$I'_0 = I_1$, I_0 is finite at zero, infinite at ∞;

$K'_0 = -K_1$, K_0 is infinite at zero, zero at ∞.

I_0 and K_0 satisfy the differential equation

[107] $\ddot{y} + \frac{\dot{y}}{x} = y.$

The Bessel function arguments have been omitted in some places below. Where the argument is not specified it is implied that

J functions have argument βa,

I functions have argument qa,

K functions have argument pa.

The easiest way to proceed is to write down the solutions for X and verify that they satisfy equations [18] and [19]. We find:

[108] $X_0 = C\, J_0(\beta r) + D\, I_0(qr),$

[109] $X_1 = E\, K_0(pr) + F\, r\, K_1(pr),$

[110] $$q^2 = (1/L_0^2) + m^2.$$

Substitution from [108] in [18] gives

[111] $$C = \frac{\tau_0 A}{\kappa^2 L_0^2 + 1}$$

where τ_0 is the value of τ for thermal neutrons in the tank. Substitution from [109] in [19] gives

[112] $$F = \tau_1 BQ/2pL_1^2$$

where τ_1 is the value of τ for thermal neutrons in the reflector. The coefficients D and E are fixed by continuity of current and density at $r = a$. Assuming equal diffusion coefficients we find:

[113] $$D = \frac{ap\,(K_1^2 - K_0^2)\,F}{pI_0K_1 - qK_0I_1}.$$

T can now be evaluated from equation [17]. Omitting factors common to $\int X$ and $\int \rho$, we have

$$\int X\,dv = \frac{C}{A}\int \rho_0\,dv + D\int_0^a r\,dr\;I_0(qr);$$

therefore

$$T = \frac{C}{A} + \frac{D}{A}\,\frac{\int_0^a r\,dr\;I_0(qr)}{\int_0^a r\,dr\;J_0(\beta r)} + \tau_{f0}$$

$$= \frac{C}{A} + \frac{D}{A}\,\frac{\beta I_1(aq)}{qJ_1(a)} + \tau_{f0}$$

$$= \frac{\tau_0}{\kappa^2 L_0^2 + 1} + \frac{\tau_0 Qa\beta^2}{2pqL_0^2}\,\frac{1 - (K_0/K_1)^2}{(pI_0/I_1) + (qK_0/K_1)} + \tau_{f0}$$

or

[114] $$T = \tau_f + \tau_t\left[\frac{1}{1 + \kappa^2 L_0^2} + \frac{Qa\beta^2}{2pqL_0^2}\,\frac{1 - (K_0/K_1)^2}{(pI_0/I_1) + (qK_0/K_1)}\right].$$

Formula for $k_e - 1$

Following the method of section 2, we express the critical condition [106] in terms of the α and λ of section 2:

$$(\alpha^2 - m^2)^{\frac{1}{2}}\,\frac{J_1[a(\alpha^2 - m^2)^{\frac{1}{2}}]}{J_0[a(\alpha^2 - m^2)^{\frac{1}{2}}]} = (\lambda^2 + m^2)^{\frac{1}{2}}\,\frac{K_1[a(\lambda^2 + m^2)^{\frac{1}{2}}]}{K_0[a(\lambda^2 + m^2)^{\frac{1}{2}}]}$$

from which we obtain the differential relation (omitting Bessel function arguments as before)

[115] $$\alpha\,\delta\alpha\left[1 + \left(\frac{J_1}{J_0}\right)^2\right] = \lambda\,\delta\lambda\left[\left(\frac{K_1}{K_0}\right)^2 - 1\right].$$

Substituting from [21] and [22] for $\delta\alpha$ and $\delta\lambda$ gives

$$\frac{k_\infty - k'_\infty - \omega(\tau_c + \alpha^2(L_f\tau_t + L^2\tau_f)]}{M^2 + 2\alpha^2 L_f{}^2 L^2} = \frac{(K_1/K_0)^2 - 1}{(J_1/J_0)^2 + 1} \frac{\omega\tau_1}{L_1{}^2}.$$

Replacing $\tau_1/L_1{}^2$ by τ_t/L^2 (equal thermal diffusion coefficients) and ω by $(k_e - 1)/T$ gives

$$k_\infty - k'_\infty = \frac{k_e - 1}{T}\left[\tau_c + \alpha^2(L_f{}^2\tau_t + L^2\tau_f) + \frac{\tau_t}{L^2}(M^2 + 2\alpha^2 L_f{}^2 L^2)\frac{(K_1/K_0)^2 - 1}{1 + (J_1/J_0)^2}\right].$$

The first term predominates over the two other terms. Since $\tau_f \ll \tau_t\alpha^2L^2 \ll 1$ and $L \doteq L_f$, we can put (replacing α^2 by κ^2)

$$[116] \qquad \frac{k_\infty - k'_\infty}{\tau_c} \doteq \frac{k_e - 1}{T}\left[1 + \kappa^2 L_f{}^2 + \frac{M^2}{L^2}\frac{(K_1/K_0)^2 - 1}{(J_1/J_0)^2 + 1}\right].$$

ACKNOWLEDGMENT

This work was described in a secret report CRT-372 (Chalk River Laboratories Atomic Energy Project, April 1948) which has recently been declassified. It is a pleasure to acknowledge many helpful discussions with B. W. Sargent and A. G. Ward.

REFERENCES

1. BAYLY, J. G. Can. J. Phys. 31: 182. 1953.
2. FERGUSSON, G. J. and GILBERT, C. W. Chalk River Report CRP-377. 1948.
3. GLASSTONE, S. and EDLUND, M. C. The elements of nuclear reactor theory. D. Van Nostrand Company Inc., New York. 1952.
4. GOODMAN, C. *Editor*. The science and engineering of nuclear power. Vol. II. Addison-Wesley Press Inc., Cambridge, Mass. 1947.
5. JOHNS, M. W. and SARGENT, B. W. Chalk River Report CRP-355. 1947. To be published.
6. RUMSEY, V. H. Chalk River Report CRP-316. Jan. 1947. To be published.

DEPENDENCE OF INTEGRATED DURATION OF METEOR ECHOES ON WAVELENGTH AND SENSITIVITY[1]

By D. W. R. McKinley

ABSTRACT

The reflecting properties of short-duration and long-duration echoes from meteor trails are examined. For short-duration echoes only, the observed relation between relative numbers and durations of meteor echoes is independent of wavelength, the time of day, or the presence of a strong shower. Integrated duration times are determined from back-scatter experiments on 9.22 m., 5.35 m., and 2.83 m., and are found to vary with the 3.5th power of the wavelength, for either short- or long-duration echoes. The integrated echo power depends on the 6th power of the wavelength. The effect of changing the equipment sensitivity is considered. The data from the back-scatter observations are used to predict the integrated duration times in the forward-scatter case, and in particular, it is shown that the results of the Cedar Rapids – Sterling very-high-frequency experiment may be explained by meteoric reflections.

INTRODUCTION

Investigations at Stanford University (2, 11, 12) have shown that reflections from meteoric trails can support, intermittently, high frequency radio transmissions well beyond the line-of-sight, without the aid of the usual E or F layer reflections. The Stanford workers have developed a theory of this forward-scatter transmission, confirmed by some experimental evidence, which indicates that the forward-scatter echo duration, T_F, can be many times as long as the back-scatter duration, T_B, provided that the trail axis is suitably oriented in each case. If 2ϕ is the angle between the incident and reflected ray, they show that $T_F/T_B = \sec^2\phi$, and this effect should greatly increase the percentage of time during which forward transmission can be supported as compared to back-scatter or normal radar reflections.

In their analysis, the Stanford workers have assumed that each meteor trail is a long, thin, ionized cylinder, enduring for not more than a second or so, hence the reflection is highly dependent on the orientation of the meteor trail. The trail should be tangent to one of a family of confocal ellipsoids, having the transmitting and receiving stations as foci. If the trail also lies in a plane containing the two stations, the amplitude of the forward-scattered signal is increased by sec ϕ, which is an additional factor favoring forward transmission.

In this paper we shall use some of the back-scatter echo data obtained at Ottawa to establish a relation between the wavelength and the integrated echo duration time. From this, a similar relation may be computed (based on some simplified assumptions) and used to predict the performance in the forward-scatter case. First, it will be pointed out that while the scattering from short-duration trails is usually highly directional, the long-duration echoes tend to lose this aspect sensitivity.

[1] *Manuscript received March 10, 1954.*
Contribution from the Radio and Electrical Engineering Division, National Research Laboratories, Ottawa, Canada. Issued as N.R.C. No. 3305.

ASPECT SENSITIVITY

We have no experimental data on long-range (500–1000 km.) point-to-point communication via meteoric ionization. We do have observations of forward-scatter over a very short base line, obtained during a couple of hours in the evening of Aug. 11, 1949, when the Arnprior and Carleton Place radar stations were inadvertently operating on nearly the same frequency, 33 Mc./sec.,

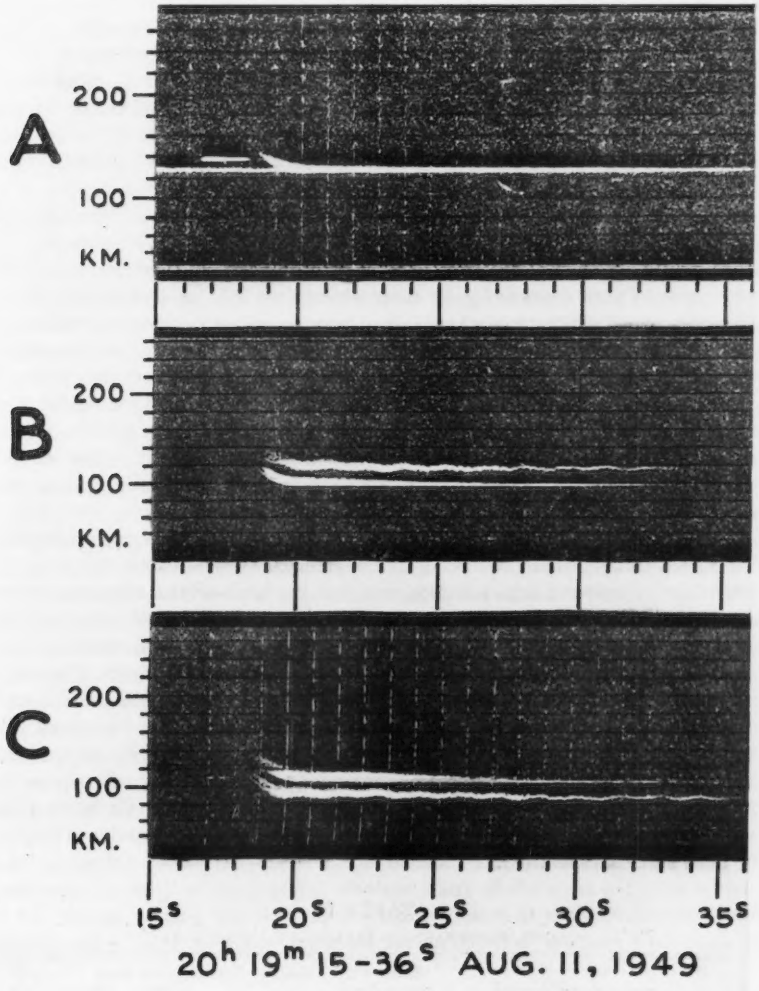

FIG. 1. Range-time record of meteor echoes at Ottawa (A), Arnprior (B), and Carleton Place (C), Aug. 11, 1949. The forward-scatter echoes on the Arnprior and Carleton Place records undulate slightly in range.

which was also close to the frequency of the Ottawa radar. The transmitters at Arnprior and Carleton Place each radiated 50 kw. pulses, at a rate of 120 per sec., locked to the common 60-cycle mains supply. Consequently, when the phasing of the two modulators happened to be suitable within narrow limits, the display at each station would show not only the normal back-scatter echo but also a quasi-stationary forward-scatter echo from the other station. The Ottawa transmitter was keyed by a nonsynchronous modulator at about 118 pulses per second, hence the echoes from Ottawa appeared on the displays at the other two stations as vertical streaks about a second apart.

Fig. 1 shows a typical *Ahb* echo recorded at all three stations on 9.2 m., at $20^h\ 19^m\ 18^s$, Aug. 11, 1949. The forward-scatter echoes can easily be distinguished from the back-scatter echoes on the Arnprior and Carleton Place records by the small sinusoidal wobble in range, presumably caused by a slight phase variation in the 60-cycle mains between the two stations.

The interstation distances are: Ottawa–Arnprior 57 km., Arnprior – Carleton Place 36 km., Carleton Place – Ottawa 41 km. These distances are far too short to enable us to draw any conclusions about the $\sec^2\phi$ effect; one would not expect T_F to exceed T_B by more than 1 or 2% for this reason alone. However, if we select meteor trails that have produced back-scatter echoes at each station, then we may expect the average T_F to be significantly greater than the average T_B. This follows if we assume line-type scattering, with the geometrical consequence that the scattering point on the trail for the forward transmissions will be located between the two back-scatter points. As the ionization density along a typical meteor trail decreases at either end of the trail, the density at the forward-scatter point will tend to be greater than the mean of the densities at the two back-scatter points.

The Arnprior and Carleton Place transmitters were locked in suitable phase for a total time of about two hours in the interval $19^h\ 20^m$ to $22^h\ 30^m$, Aug. 11, 1949. The criterion of echo selection was that the back-scatter echoes appeared at all three stations, making sure in the case of very-short-duration echoes that the relative times of initial appearances were consistent with the trail geometry. For the present purpose, only the Arnprior and Carleton Place data are used, but the Ottawa radar range was needed for triangulation and path determination of selected meteors. Table I summarizes the data for echoes with back-scatter durations less than one second at either Arnprior or Carleton Place, and for echoes with durations over four seconds. For each meteor the forward-scatter durations measured at both Arnprior and Carleton Place were averaged, and similarly the mean of the back-scatter durations observed at both stations was used.

TABLE I

T_F/T_B = RATIO OF FORWARD- TO BACK-SCATTER ECHO DURATION

	Echoes less than 1 sec.	Echoes more than 4 sec.
Number of meteors	14	10
T_F/T_B	1.48	1.02

The number of observations is small because of the stringent selection conditions but the results are nevertheless statistically significant. Without exception the mean T_F was greater than the mean T_B for each of the short-duration echoes, while for the long-duration echoes the mean T_F varied only a few per cent, one way or the other, from the mean T_B in each case. Since the $\sec^2\phi$ effect is negligible in our experiment, the 50% increase in T_F over T_B for short-duration echoes can reasonably be explained qualitatively by assuming that the short-duration echoes come from long, thin columns of ionizations that are less highly ionized near the ends.

The approximate equality of T_F and T_B for the long-duration echoes could imply that the ionization density at the back-scatter points on the trail is about the same as that near the middle. This may not seem unreasonable at first glance, if one considers that large meteors may create trails 100 km. or so long, and that there could be less variation in the density per km. for a selected 20 km. segment than in the case of a small meteor with an overall trail length of 30 km. However, it was observed that for *F*-type echoes lasting a few seconds the appearances of the echoes on each display were usually simultaneous (i.e. within 0.05 sec., which was the limit of time resolution between stations), in contrast to the easily measurable delays observed in the case of the short echoes. The implication appears to be that all stations simultaneously receive an echo from the same point or "hot-spot" on the trail. This "hot-spot" could be either a sudden distortion in a uniform trail (3), or a short segment of denser ionization (7). Evidence from the simultaneous doppler station records confirms this impression; most of the selected short echoes showed the first Fresnel zone while very few of the longer echoes did.

The *Ahb* echo types, an example of which appears in Fig. 1, show the simultaneous appearance of the echoes at the three stations. In other *Ahe*-type echoes there may be several seconds delay between the appearance of the *h*-echo and the various *e*-characteristics, but separate triangulation of the *e* components shows that they arise from discrete points on the original trail, and therefore that the scattering from these points must be substantially non-directional. The *h*-characteristic corresponds closely to the path of the moving meteoroid. Every meteor echo occurring near t_0 may be said to have an associated head echo, caused by diffraction scattering from the forming trail, both when approaching and receding from the observer, but only for the brighter echoes can an appreciable change in range be detected. The rapid decrease in signal strength on either side of t_0 is in agreement with the diffraction theory in these cases. In other cases the behavior of the head echo suggests a "moving ball" of ionization at the head of the meteor. The diffraction echo has its maximum intensity at the t_0 point, whereas many of the observed head echoes do not behave in this manner and are more consistent with the moving ball type of target, with an echo amplitude independent of position with respect to t_0.

The highly-directive properties of the short-duration echoes and the non-directive characteristics of the long-duration echoes were shown statistically in a previous paper (6) by analyzing the short and long echo rates during the

Perseid shower as the radiant rose. When the radiant elevation passed 60° the short-duration echo rates fell off rapidly because the R_0 ranges, corresponding to the t_0 points, exceeded the maximum recorded range. On the other hand, the number of long-enduring echoes steadily increased, roughly as the sine of the radiant elevation angle, as one would expect if these echoes were independent of trail aspect.

To sum up, it is seen that the short-duration echoes, say those less than two or three seconds on 9.22 m., behave as if the meteoric target were a line scattering source, and hence have predictable directional characteristics. Echoes of longer duration tend to lose this aspect sensitivity and echoes more than 10 sec. long may, on the average, be expected to scatter energy in all directions, and some may do so at the first instant of their appearance.

There is little in the discussion so far that is new, as the intention has been to emphasize from previous knowledge the difference in the reflecting properties of long- and short-duration meteor echoes. In an earlier paper (7) we postulated the presence of "blobs" of denser ionization along the trail in an attempt to account for some of the long-enduring echoes. Greenhow (3) has criticized our hypothesis on the basis that if the blob theory were correct the echoes should be detected by a short-wave radar before being seen by a long-wave radar, and experiments show that this does not occur, in general. Greenhow postulates that the equipment sensitivities should be adjusted as the inverse third power of the wavelength, which we believe to be prejudging the issue, i.e., to be equivalent to assuming that long-duration echoes have the same properties as short-duration echoes. However, if we accept this arbitrary sensitivity ratio it does follow that a smaller target area is required to produce the minimum detectable echo on the shorter wavelength; hence, as the blob expands it should be seen first on the short-wave set. The flaw in the argument is the assumption that, at a given instant, the meteor target must present the same effective dimensions to both radars. That is, the electron density across a diameter of the blob would have to be constant, with an abrupt discontinuity at the boundary. Owing to radial diffusion this is an unrealistic picture; several better models have been suggested, and, for example, a gaussian gradient of density seems more appropriate. As the critical density is inversely proportional to the square of the wavelength, it follows that the effective target area presented to the long-wave set may be considerably greater than for the short-wave set. The actual values depend on the particular model chosen, but an analysis of several reasonable hypotheses indicates that the ratio of the target areas can be more than sufficient to ensure that the long-wave echo is stronger, despite the inferiority in equipment sensitivity.

BACK-SCATTER INTEGRATED ECHO DURATIONS

In an earlier paper (6) we presented some statistics of back-scatter echo durations as observed in pairs simultaneously on 9.22 m. and 5.35 m., and on 9.22 m. and 2.83 m. We can use these data directly to determine the integrated durations on 5.35 m. and 2.83 m., but a further reduction of the 9.22 m. records will be needed because many meteors detected on this wavelength did not

appear on the shorter wavelength displays. The discussion in the previous section suggested that an arbitrary value of two or three seconds might be chosen as a dividing line for the two groups of 9.22 m. echo durations. On the average the durations on 5.35 m. and 2.83 m. will be only 1/3 and 1/10, respectively, of the 9.22 m. durations for the same meteors. Therefore, we shall divide the 9.22/5.35 m. data of Ref. 6 into echoes less than 1 sec. and echoes 1 sec. and over, and the 9.22/2.83 m. data of Ref. 6 into echoes less than 0.4 sec. and those greater.

We define D as the total echo duration divided by the total observing time; D may be expressed as a fraction (which may exceed unity) or in seconds per hour, or as a time percentage. $D = \sum_n N_n T_n$, where N_n is the number of echoes of duration T_n. D_B and D_F will refer to the back-scatter and forward-scatter cases respectively. Letters in brackets following the symbols will be used where it is desirable to distinguish between the echo groups, as follows: (S) short echoes, (L) long echoes, (A) all echoes. D' will be used for the fractional time during which at least one echo is present. D' will in general be less than D and will never exceed unity.

Table II here summarizes all data from Table III, Ref. 6; Table III the data for Film No.'s 4 and 7 only, from Table V, Ref. 6; Table IV all data from Table VI, Ref. 6; and Table V all data from Table II, Ref. 6. The normalized hourly durations are the observed durations multiplied by a correction factor to equate the system parameters of the 5.35 m. and 2.83 m. sets to that of the 9.22 m. standard equipment. This factor will be derived later in the section on the variation of D with system sensitivity. In applying it here, allowance is made for the fact that the increase in duration with a given increase in sensitivity is greater for the shorter echoes (5), and slightly different factors are used for the short- and the long-duration groups.

TABLE II

5.35 M. D_B—MINIMUM PERIOD. MEAN TIME 1850 E.S.T., AUG. 1950

	$T_B < 1$ sec.	$T_B \geqslant 1$ sec.	All T_B
Observed D_B (sec./hr.)	5.9	20	26
Normalized D_B (sec./hr.)	14.5	47	62

TABLE III

5.35 M. D_B—MAXIMUM PERIOD. MEAN TIME 0430 E.S.T., AUG. 1950

	$T_B < 1$ sec.	$T_B \geqslant 1$ sec.	All T_B
Observed D_B (sec./hr.)	8.9	310	319
Normalized D_B (sec./hr.)	22	730	752

TABLE IV

5.35 M. D_B—OVER-ALL PERIOD. MEAN TIME 2330 E.S.T., AUG. 1950

	$T_B < 1$ sec.	$T_B \geqslant 1$ sec.	All T_B
Observed D_B (sec./hr.)	8.1	120	128
Normalized D_B (sec./hr.)	20	280	300

TABLE V

2.83 M. D_B—LONG-TERM AVERAGE. FEB.–APRIL 1950

	$T_B < 0.4$ sec.	$T_B \geqslant 0.4$ sec.	All T_B
Observed D_B (sec./hr.)	0.22	0.51	0.73
Normalized D_B (sec./hr.)	2.8	5.6	8.4

Counts were made of the long and short echo durations on 9.22 m. using Film No. 5 of the minimum period (Ref. 6) and Film No. 4 of the maximum period of the 9.22/5.35 m. observations, and these are listed in Tables VI and VII. Here, D_B' is significantly less than D_B, and the D_B' values may be determined directly by subtracting the measured overlaps. The overlap in most cases was of the order of 2 or 3%, but during the maximum period it amounted to 15% of D_B for the long-duration echoes.

TABLE VI

9.22 M. D_B—MINIMUM PERIOD. MEAN TIME 1850 E.S.T., AUG. 1950

	$T_B < 3$ sec.	$T_B \geqslant 3$ sec.	All T_B
Observed D_B (sec./hr.)	129	120	249
Observed D_B' (sec./hr.)	128	117	243

TABLE VII

9.22 M. D_B—MAXIMUM PERIOD. MEAN TIME 0430 E.S.T., AUG. 1950

	$T_B < 3$ sec.	$T_B \geqslant 3$ sec.	All T_B
Observed D_B (sec./hr.)	227	1358	1585
Observed D_B' (sec./hr.)	223	1160	1365

Except for Table VI, the tables show that $D_B(L)$ is greater than $D_B(S)$, and the ratio increases as the shower radiant rises. This depends to some extent, of course, on the selected dividing lines between the groups but it is not very sensitive to the choice of these lines, within reasonable limits.

On Film No. 5 (Table VI) the 9.22 m. part of the record showed a meteor echo lasting 38 min. which did not appear at all on 5.35 m. This is the longest duration that we have noted in our records; it was overlooked in a previous paper on long-duration echoes (8). This exceptionally long echo has been deleted from the data of Table VI, as its inclusion would have seriously upset the statistics. The echo extended from 200 km. to 260 km. for much of its life and hence will have obscured some normal echoes. The masking would be more severe for the long-duration group than for the short-duration echoes, as the latter echoes tended to occur at short ranges in this period.

DEPENDENCE OF D_B ON WAVELENGTH

To determine the wavelength dependence of D_B the experiments in the previous section should ideally have been done with all three radars simultaneously. Or, lacking this, the 9.22/5.35 m. and the 9.22/2.83 m. records

should each have covered a shower period and a nonshower period. Regrettably, the 9.22/5.35 m. data are available only for the period of the Perseid shower, and the 9.22/2.83 m. data were observed over many days in which no strong showers occurred. Fortunately, the mean of all the 9.22/2.83 m. records may be taken to represent the average performance, around the clock during nonshower conditions, and a period when similar average conditions existed may be selected from the 9.22/5.35 m. information. On a 24-hr. basis the average nonshower echo rate of the 9.22 m. radar has been established to be about 400–500 echoes per hour. A plot of hourly echo rates versus time showed that the 9.22 m. over-all rates were about 450 echoes per hour in the neighborhood of 2100 E.S.T. during the August period. Interpolation of the D_B data in the tables above was then employed to deduce D_B values for 9.22 m. and 5.35 m. at 2100 E.S.T. These values, together with the 2.83 m. normalized figures, will be adopted as averages for mean standard or nonshower conditions; they are given in Table VIII.

TABLE VIII

ADOPTED AVERAGE D_B FOR DIFFERENT WAVELENGTHS

λ, m.	D_B(S), sec./hr.	D_B(L), sec./hr.	D_B(A), sec./hr.
9.22	150	400	550
5.35	18	100	118
2.83	2.8	5.6	8.4

The data of Table VIII are presented in Fig. 2 by plotting the common logarithm of D_B, expressed in sec./hr., against the logarithm of the wavelength in m. For convenience, scales in Mc./sec. and percentage of time have been

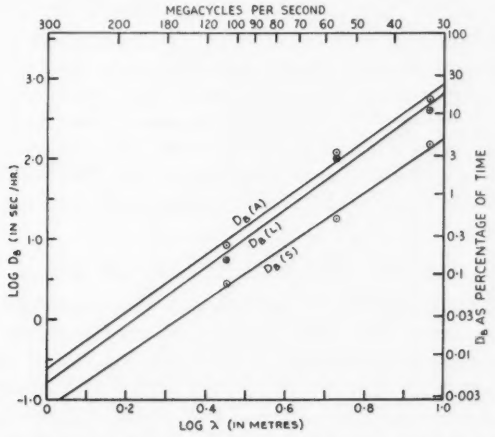

FIG. 2. Observed values of log D_B(S), log D_B(L), and log D_B(A) for three wavelengths, 9.22 m., 5.35 m., and 2.83 m. Back-scatter case under average conditions.

added to Fig. 2. The three straight lines have been fitted by least squares, and have the following equations:

$$[1] \qquad \begin{aligned} D_B(S) &= 7.9 \times 10^{-2}\lambda^{3.36}, \\ D_B(L) &= 15.4 \times 10^{-2}\lambda^{3.64}, \\ D_B(A) &= 23.7 \times 10^{-2}\lambda^{3.55}, \end{aligned}$$

where λ is in meters and D_B in sec./hr.

The exponent of λ depends here on our selection of 9.22 m. and 5.35 m. observing periods, but it is not very sensitive to this choice. For example, the range $400 < D_B(A) < 700$ sec./hr. for 9.22 m. echoes yields the spread $\lambda^{3.3} < \lambda^n < \lambda^{3.8}$. We may therefore conclude that the fractional time during which back-scatter reflections are obtainable is proportional to an exponent of the wavelength that is greater than the 3rd power but is not likely to exceed the 4th power.

For convenience in our later discussion we shall adopt 3.5 as the power of λ for all three lines in Fig. 2. The proportionality factors in Eqn. 1 will also require some readjustment, which will be based on the approximate values read from the graphs at $\lambda = 5$ m. The adjusted set of equations is:

$$[2] \qquad \begin{aligned} D_B(S) &= 5 \times 10^{-2}\lambda^{3.5}, \\ D_B(L) &= 15 \times 10^{-2}\lambda^{3.5}, \\ D_B(A) &= 20 \times 10^{-2}\lambda^{3.5}. \end{aligned}$$

The relative values of the proportional factors for $D_B(L)$ and $D_B(S)$ depend on the arbitrary choice of the dividing lines for the short- and long-duration groups. Using different dividing lines in the range $1 < T_B < 6$ sec. on 9.22 m., it is found that the ratio $D_B(L)$: $D_B(S)$ is still above 2: 1 but is unlikely to be higher than 4: 1.

We do not have data for wavelengths longer than 9.22 m., but the experience of the Stanford workers suggests that the lines of Fig. 2 might be extrapolated with confidence up to $\lambda = 20$ m. or more. As D_B (expressed as a fraction) approaches and exceeds unity D_B' will approach unity. An elementary analysis, based on probability theory, suggests that if the meteors occur at random, $D_B' = 1 - \epsilon^{-D_B}$. However, the problem is complicated by the observation that the fainter visual meteors tend to occur more frequently in groups, rather than being distributed entirely at random (9). This has been confirmed for radar meteors by some unpublished analysis in progress at Harvard, using our radar records.

METEOR NUMBERS AND ECHO DURATION

In Fig. 3 we have plotted the logarithm of relative numbers of echoes (not corrected hourly rates) against the mean logarithm of the duration, for 5.35 m. echoes. The circled points are taken from Table III, Ref. 6, and represent a period of minimum background and shower activity, i.e., 1630–2110 E.S.T., during the Perseid shower. The crossed points are taken from Table V, Ref. 6, and represent a period of high activity for all background meteors and the long-duration shower meteors (0210–0650 E.S.T.). The solid straight line has

been drawn through the circled points, with a measured slope $m = -0.74$. The dashed straight line was fitted to the short-duration points only of the crossed points; its slope is $m = -0.82$. The long-duration groups of the maximum period deviate considerably from the dashed straight line because there were a large number of long Perseid echoes in this period but relatively few short-duration Perseids.

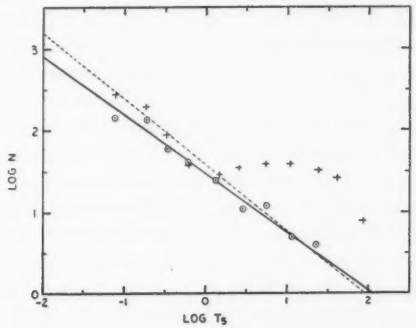

FIG. 3. Relation between the logarithm of the relative numbers of echoes and the logarithm of their durations, observed on 5.35 m. The circled points and solid line represent the minimum period, 1630–2110 E.S.T., of the Perseid shower, and the crossed points and dashed line represent the maximum period, 0210–0650 E.S.T., Aug. 11–13, 1950.

In Fig. 4, similar relations between relative numbers and durations are shown, using the 9.22 m. data, which are summarized in Tables VI and VII of this paper, but not tabulated in detail. The circled points refer to the minimum period, 1630–2115 E.S.T., and the crossed points to the maximum period, 0207–0657 E.S.T. Two straight lines have been drawn through the

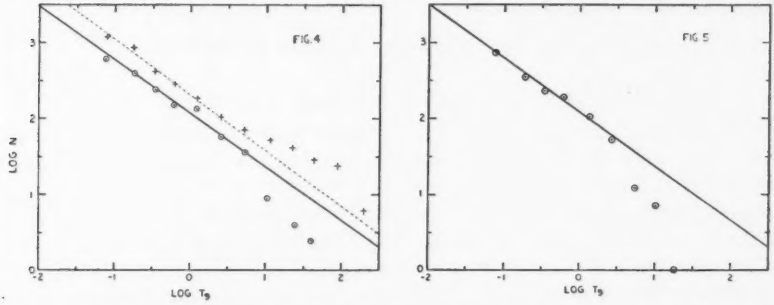

FIG. 4. Relation between the logarithm of the relative numbers of echoes and the logarithm of their durations, observed on 9.22 m. The circled points and solid line represent the minimum period, 1630–2115 E.S.T., of the Perseid shower, and the crossed points and dashed line represent the maximum period, 0207–0657 E.S.T., Aug. 12–13, 1950.

FIG. 5. Relation between the logarithm of the relative numbers of echoes and the logarithm of their durations, observed on 9.22 m. The observations were made during two nonshower periods, 2230–0130 E.S.T., June 14/15 and 15/16, 1950.

short-duration groups for each period, and again it is seen that the long-duration groups deviate from the respective lines. The slope of the solid line (minimum period) is $m = -0.72$, and that of the dashed line (maximum period) is $m = -0.74$.

Fig. 5 shows the log N/log T relation for an average nonshower period. The data were taken from the 9.22 m. records for June 14/15 and June 15/16, 1950, 2230–0130 E.S.T. The slope of the line drawn through the short-duration echoes is $m = -0.72$. The long-duration echoes fall below the line in this case. It appears that during periods of little activity the slope of the log N versus log T graph for long echoes becomes more negative than the slope of the short-duration graph, and during periods of peak activity the slope becomes more positive. The long-duration echoes are the ones more usually correlated with visual meteors. Hence, anomalous conclusions may be drawn, unless care is exercised, if one were to attempt to compare these log N/log T relations directly with Millman's log T/M graph (10), combined with the log N/M relation given in a previous paper (4), where M is the visual magnitude.

It is seen that the slope of the log N versus log T relation is practically independent of echo rates and wavelength, if we confine our attention to the short-duration echoes. We shall adopt a slope $m = -0.75$ as representative. If it had happened that $m = -1$, then all groups would have had the same duration sum, analogous to the relation of constant mass per magnitude interval given by Watson (13).

We have used a scale of 2 for the duration groups (or nearly so for the very short echo groups), i.e., $T_n = T_{n-1}/2$. From above, $N_n = KT_n{}^m$, where $m = -0.75$. If S_n is the over-all number of meteors from the largest observed T down to T_n, then

$$S_n = \sum_n N_n = KT_n{}^m \sum_{p=0}^{\infty} 2^{pm} = N_n/(1 - 2^m) = 2.5N_n, \text{ for } m = -0.75.$$

The integrated echo duration is

$$D = \sum_n N_n.T_n = K\sum_n T_n{}^{m+1}, \text{ where } m + 1 = 0.25.$$

VARIATION OF D WITH SYSTEM SENSITIVITY

Let the sensitivity of our standard system be varied by changing the transmitter power or the receiver bandwidth, keeping the wavelength constant. We define the sensitivity factor x as the logarithm of the power sensitivity ratio. It has been found that the over-all echo rates vary as the square root of the sensitivity ratio (4), or log $S_n \sim x/2$. From above, if S_n is doubled, by means of a four-fold increase in power for example, it follows that each N_n will also be doubled. Furthermore, every echo that was recorded before will be increased slightly in duration (5), the increase being greater for the short-duration echoes. Both effects will increase D, but the increase in numbers is more important.

In our work an arbitrary lower limit of resolution $T = 0.05$ sec. has been set. No doubt there are myriads of echoes shorter than this on the records

but they tend to be indistinguishable from noise spots, which are of the order of 0.02 sec. This is simply a mechanical limitation of the recording system; the wide bandwidth of 250 kc./sec. will inherently allow very much better resolution, but we are limited by the spot size on the cathode ray tube and the 120 c.p.s. sampling frequency. Our doppler records, for example, although using lower power and narrower bandwidth, have a resolution of a millisecond or better. For purposes of this discussion a minimum $T = 0.05$ sec. for any sensitivity factor will be assumed. This means that if the sensitivity is increased, more echoes will appear in the group $T = 0.05$–0.10 sec., and those that were there will increase in duration, with many of them now falling within the next group. If T_0 is the dividing line for short- and long-duration echoes on our standard system some of the echoes in the group below T_0 will pass over above T_0. These are still echoes from directional trails and should be included in $D(\mathrm{S})$. Because of the fixed lower limit to T the range of summation for $D(\mathrm{S})$ will thus increase or decrease with x. A similar increase in numbers and durations will be observed for the long echoes, and the range of summation will again vary slightly with x.

For our standard system we have computed $N_n T_n = K T_n^{0.25}$ from the experimental data for each interval of log $T = 0.301$ in the range $-1.20 <$ log $T < 2.10$. The summation for $D(\mathrm{S})$ extended over the first five groups to log $T = 0.30$, corresponding roughly to our selected T_0, and the summation of $D(\mathrm{L})$ included the remainder. The sensitivity ratio was then increased by a factor 100, for example, which increased the numbers in each group by 10 and added a new group to $D(\mathrm{S})$ because the mean T had been increased by a factor of 2. The number of groups in the $D(\mathrm{L})$ summation remained the same by creation of a new group beyond log $T = 2.10$.

Fig. 6 shows the relative values of $D_{\mathrm{B}}(\mathrm{S})$ and $D_{\mathrm{B}}(\mathrm{L})$, computed in this manner and plotted against x. The graphs are not quite straight lines but mean

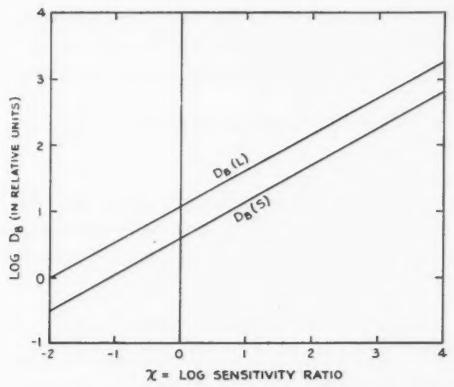

FIG. 6. Computed relative values of log $D_{\mathrm{B}}(\mathrm{S})$ and log $D_{\mathrm{B}}(\mathrm{L})$ plotted against the logarithm of the sensitivity ratio.

straight lines can be fitted to either curve and each has the slope 0.56. Hence, we have

$$[3] \qquad \log D \text{ (System II)} = 0.56\, x + \log D \text{ (System I)},$$

where x is the log of the sensitivity ratio of System II to System I. Inclusion of the effect of increased duration has thus raised the exponent of the sensitivity factor from 0.50 to 0.56.

Our standard system has a peak power of 200 kw. (average power 5 kw.), antenna gain 3.5, minimum detectable signal 2×10^{-14} watts in a receiver bandwidth 250 kc./sec., and is assumed to use any wavelength between 2 m. and 10 m. If a bandwidth of 1 kc./sec. were acceptable, for example, the peak power could be reduced to 0.8 kw. with the same sensitivity, though with some depreciation of the resolution, or the rate of transmission of intelligence. However, it has been assumed so far that the echo reflections were usable down to receiver noise level, which is undesirable for practical purposes. If signals 10 db. above noise are regarded as the lower working limit, one could increase the transmitter power by a factor of 10, reject all signals below 10 db., and still have the same D. Or, alternatively one could leave the system parameters fixed and use only echoes rising 10 db. above noise. Here $x = -1$ and the new D is $10^{-0.56} = 0.28$ times the original D. Referring to Fig. 2 this would mean that the usable back-scatter transmission times would be divided by 4, anywhere on the chart.

RELATION BETWEEN INTEGRATED ECHO POWER AND WAVELENGTH

From Equation 2, we have for any two selected values D_2 and D_1,

$$[4] \qquad \log D_2 - \log D_1 = 3.5\, (\log \lambda_2 - \log \lambda_1).$$

From Equation 3, we may write,

$$[5] \qquad \log D_2 - \log D_1 = 0.56\, x = 0.56\, (\log P_2 - \log P_1)\,,$$

where P_2 and P_1 are, for example, the two transmitter powers on a given wavelength that will yield the same D_2 and D_1 that would be obtained with equipments of identical sensitivity operating on wavelengths λ_2 and λ_1, as given by Equation 4.

From Equations [4] and [5] we may eliminate D_2 and D_1, hence,

$$[6] \qquad P \sim \lambda^{6.3}.$$

Thus, in order to maintain D at a selected value the sensitivity must vary as the sixth power of the wavelength. If the system sensitivity is held constant then Equation [6] also indicates that the integrated echo power will vary as the sixth power of the wavelength.

THE FORWARD-SCATTER CASE

The results of the back-scatter experiments may be employed to suggest the probable performance when the transmitter and receiver are separated by the order of 1000 km. Eshleman and Manning (2) have developed a theory of the probability of detecting randomly oriented trails over such a path. Meteor

trails are not distributed randomly, certainly not in their space orientations, and possibly not in time. The distributions of the known meteor radiants are very complex, and, as will be seen later, the meteors contributing to the forward-scatter case may be several magnitudes smaller than the meteors that have been studied hitherto and their distributions are unknown. We therefore hesitate to attempt to extend the Stanford analysis to a more general case that might be a better representation of actual conditions. In fact, for the purposes of the following discussion we shall greatly simplify the working assumptions, and avoid probability theory and meteor distributions as much as possible.

Following the Stanford experience we shall simply assume that the observed $D_B(S)$ may be multiplied by a factor greater than unity, based on the $\sec^2\phi$ effect mentioned earlier, in order to yield a computed $D_F(S)$. Villard *et al.* (11) found for reflection at the mid-point of a 1175 km. path that $T_F/T_B = 23$. The average ratio for all distinguishable echoes was 4.5, which included many cases where the reflection point was near one station and $\sec^2\phi$ was therefore much smaller. We shall assume that directional antennas will be used, to illuminate only a region in the vicinity of the mid-point. Thus, on the average, the T_F/T_B ratio should be intermediate between the above two observational values. We shall adopt representative multiplying factors, $f(S) = 5$, 10, and 15. The amplitude factor, proportional to sec ϕ, will also operate in favor of increased $D_F(S)$, but we shall omit this for the moment. $D_B(L)$ will not be increased by the $\sec^2\phi$ effect as much as $D_B(S)$, but the forward-scatter durations should certainly be increased by some factor because many of the long-duration trails will have retained some directional characteristics. Arbitrarily, we shall assume representative factors $f(L) = 2$, 4, and 6.

Three computed graphs of $D_F(A)$ versus wavelength are shown in Fig. 7.

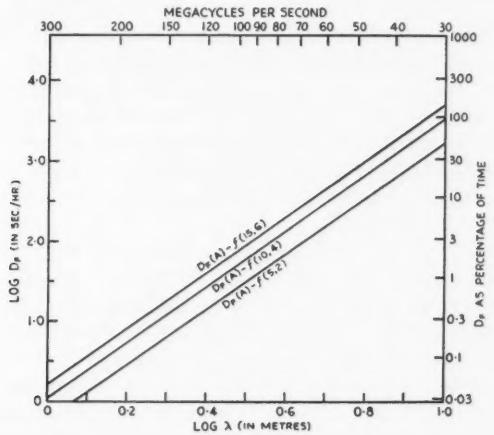

FIG. 7. Computed graphs of log $D_F(A)$ as a function of wavelength, for three arbitrary sets of multiplying factors, $f(5, 2)$, $f(10, 4)$, and $f(15, 6)$. Forward-scatter case under average conditions.

$D_F(A)$ for $f(5, 2)$, for example, means that the calculated forward-scatter duration has been obtained by multiplying $D_B(S)$ by 5 and $D_B(L)$ by 2 and then adding the two figures. The relations of Eqn. 2 have been used as the basis. Because of the assumptions involved, the graphs of Fig. 7 should be regarded only as representative of the order of magnitude to be expected in the forward-scatter case, though it is believed that they are conservative underestimates.

The graphs of $D_F(A)$ in Fig. 7 apply to a spaced-station system using the power and sensitivity of our standard radar. The $D_F(A)$ for a system of different sensitivity and wavelength may be found by first entering Fig. 7 at the desired wavelength and then correcting the corresponding $D_F(A)$ by using Fig. 6, or the equivalent analytical formula, Eqn. 3, to adjust for the difference in system sensitivity. At a frequency of 50 Mc./sec. for example, we would expect, under average nonshower conditions with our standard system, that $D_F(A) = 8$, 16, or 24% of the time, corresponding to the assumed factors $f(5, 2)$, $f(10, 4)$, and $f(15, 6)$. During the early morning hours, with no shower present, the values would be roughly doubled, while in the early evening hours they might be halved. The presence of a strong shower might be expected to increase the time percentages further, when the radiant is favorably located with respect to the transmission path.

The geometry of the forward-scatter case differs from that of the back-scatter experiments, and an examination of some of the differences is necessary to insure that the above analysis is justified. Let us assume that the transmitter and receiver are 1000 km. apart, each using similar directive antennas with patterns illuminating the *E*-region in a large area centered above the mid-point of the stations. The effective area in the meteor region that a typical $20° \times 30°$ beam thus intersects is about the same as that intersected overhead by our back-scatter radar with a broad antenna pattern, when the recorded range is limited to 260 km. The relative numbers of meteors of a given magnitude will therefore be comparable. The forward transmission path is roughly three times the mean back-scatter path, and the attenuation with range will vary as $1/R^3$ for the short echoes and $1/R^4$ for the long echoes; the forward loss will then be 14–19 db. The antenna gain of the $20° \times 30°$ beam (measured between half-power points) is about 45, or 16.5 db., compared to the gain of 3.5, or 5.4 db., used in the back-scatter experiments. The net gain is twice the difference of these antenna gains expressed in db.; in this case the net gain will be 22 db., or more than sufficient to compensate for the range attenuation. Therefore, our estimates of D_F above may be regarded as reasonable and conservative. Admittedly, there is considerable speculation throughout in this analysis, especially in the f factors. There is no really satisfactory substitute for performing the actual experiments.

In practice, it would probably be better to direct the antenna beams to one side or the other, or to both sides (split beam) of the line joining the stations, as Eshleman and Manning have recommended (2). Only meteor trails nearly parallel to the earth's surface and to the line joining the stations will show the full benefit of the $\sec^3\phi$ and $\sec\phi$ effects, and very few of these occur. By

directing the beams to one or both sides, a greater number of suitably-oriented trails will be available from meteors with higher radiants. The long-duration echoes are not affected to the same extent by this reasoning.

THE CEDAR RAPIDS–STERLING EXPERIMENT

As another example, consider the data of a forward-scatter experiment in which the transmitter, on 49.8 Mc./sec., was located at Cedar Rapids, Iowa, and the receiver was at Sterling, Virginia (1). The parameters of this experiment, here designated System B, are compared with our standard characteristics as evaluated for the forward-scatter case, System A, and the net gain or loss is shown in Table IX.

TABLE IX

	System A, standard	System B, Cedar Rapids-Sterling	Gain in db.
Transmitter power	200 kw. (peak)	23 kw.	−10
Path distance	1000 km.	1270 km.	− 4
Antenna gain	17 db.	18 db.	+ 2
Receiver bandwidth	250 kc./sec.	16 c.p.s.	+42
		Net gain	+30 db.

The receiver bandwidth for System B has been calculated as the geometric mean of the published values of I.F. and output bandwidths, which were 3 kc./sec. and 1/12 c.p.s. respectively. Here $x = 3.0$, and therefore D_F for System B will be $48 \times D_F$ for System A. From Fig. 7 we find D_F for System A to be 8, 16, or 24%, assuming System A to be on 49.8 Mc./sec. Therefore D_F for System B will be roughly 385, 770, or 1150%, depending on the choice of the f factors. If we use the simple relation $D_F' = 1 - \epsilon^{-D_F}$, we find that $D_F' = 97.9$, 99.95, and 99.999% for the respective choices. These figures apply to signals measured down to noise level, and suggest that it is highly improbable that the signal will fall below noise level for any significant time.

For a signal level of 10 db. above noise, which appears to be a representative mean value of the signal strength recorded in System B, we multiply the D_F figures above by $10^{-1.0\times0.56} = 0.28$, to yield percentages of 108, 216, and 324 respectively. The corresponding D_F' values are 66, 88.5, and 96.1%. These should be regarded as minimum figures for average conditions, because we have ignored the contribution that will be made in System B by echoes less than 0.05 sec. duration. These may be of the order of milliseconds and still pass through the I.F. amplifier; the output filter, of course, integrates the power contributions of all echoes less than a few seconds duration. The over-all echo rate on System B will be 30 times the rate on System A, or over 200 echoes per min. of duration 0.05 sec. and longer. With a time constant of 12 sec. in the output stage of System B it is not surprising that the signal should appear to be continuous. Any gaps in D' of the order of a second or so will be smoothed out and longer gaps should be rare indeed. System B will detect meteors at least four magnitudes fainter than System A, possibly down to the 14th or

15th visual magnitude (4). The presence of the strong visual meteor showers should not affect System B as much as System A, because these showers appear to contain relatively few very small meteors.

The mean diurnal variation of signal strength published for System B is of the same general form as the typical diurnal meteor rate curve obtained with our standard back-scatter system, though there are some discrepancies. These may be due to the hitherto unknown distribution of meteors in the range 10th–15th magnitude. As far as we are aware none of the conventional high-resolution meteor systems has been able to study meteors of this magnitude. Naturally, the individual identity of the meteor echo is entirely lost in System B, except for its average power contribution. It may be that incorporating filters with long time constants in the present meteor systems will add to our knowledge of these small meteors, though the observing techniques and the analysis will have to be modified considerably.

We have shown for System B that D' should be very close to 100%. Thus, continuous communication should be obtainable, though at a low intelligence rate because of the narrow bandwidth. Intermittent communication at higher intelligence rates has often been demonstrated.* The authors of the report on the Cedar Rapids – Sterling experiment considered that the received signal was due to scattering from discontinuities in the lower E-region ionization, possibly due to the effects of turbulence. We are suggesting here that their results might be explained almost entirely on the basis of meteoric reflections. In a previous paper (8) we reported the observation on 33 Mc./sec. of a weak scatter echo at a height of about 80 km., and at that time we suggested that the agency responsible for this continuous echo might be the same as the mechanism that supported the transmissions in the Cedar Rapids – Sterling experiment. If this continuous echo were due to meteors, the range of meteoric masses must be much smaller than the usual ranges of background and shower meteors, and there can be few meteors brighter than the 9th magnitude, say. Meteoric dust clouds could be responsible. The case is not proved and we still feel that ionospheric discontinuities may offer a stronger explanation for our weak scatter echo. On the other hand, returning to the forward-scatter case, we think that meteoric reflections constitute the major contribution to the observed signal, with scattering from ionospheric turbulence as a possible secondary mechanism.

REFERENCES

1. Bailey, D. K., Bateman, R., Berkner, L. V., Booker, H. G., Montgomery, G. F., Purcell, E. M., Salisbury, W. W., and Wiesner, J. B. Phys. Rev. 86: 141. 1952.
2. Eshleman, Von R. and Manning, L. A. Proc. Inst. Radio Engrs. 42: 530. 1954.
3. Greenhow, J. S. Proc. Phys. Soc. (London), B, 65: 169. 1952.
4. McKinley, D. W. R. Can. J. Phys. 29: 403. 1951.
5. McKinley, D. W. R. Can. J. Phys. 31: 758. 1953.
6. McKinley, D. W. R. Can. J. Phys. 31: 1121. 1953.
7. McKinley, D. W. R. and Millman, P. M. Proc. Inst. Radio Engrs. 37: 364. 1949.

* *Fig. 1 illustrates intermittent meteor communication with the extremely wide intelligence bandwidth of 250 kc./sec. Amateur radio operators for years have used meteors for transient communication of speech frequencies, although they may not always have been fully aware of the agency involved. More recent data (unpublished) indicate that even the f(15, 6) line on Fig. 7 is a minimum estimate of the meteoric forward-scatter performance, rather than a maximum.*

8. McKINLEY, D. W. R. and MILLMAN, P. M. Can. J. Phys. 31: 171. 1953.
9. MILLMAN, P. M. J. Roy. Astron. Soc. Can. 30: 338. 1936.
10. MILLMAN, P. M. J. Roy. Astron. Soc. Can. 44: 209. 1950.
11. VILLARD, O. G., PETERSON, A. M., MANNING, L. A., and ESHLEMAN, VON R. J. Geophys. Research, 58: 83. 1953.
12. VILLARD, O. G. and PETERSON, A. M. QST, 37: 11. 1953.
13. WATSON, F. G. Between the planets. 1st ed. The Blakiston Co., Philadelphia, Penn. 1941. p. 115.

AN EXPERIMENTAL STUDY OF BAND INTENSITIES IN THE FIRST POSITIVE SYSTEM OF N_2

I. VIBRATIONAL TRANSITION PROBABILITIES[1]

By R. G. Turner and R. W. Nicholls

ABSTRACT

Integrated intensities of 52 bands of the N_2 first positive system have been measured using a recording infrared spectrometer. These data have been interpreted as vibrational transition probabilities which were compared with theoretical values calculated under the assumption that the electronic transition moment is independent of internuclear separation. The comparison shows that the assumption is not valid for this electronic transition.

INTRODUCTION

Accurate measurements of intensities of molecular spectra have to a large extent been neglected in comparison with the establishment of accurate wavelengths and energy level assignments. However, in the study of physical conditions of molecular excitation existing in spectroscopic sources of both terrestrial and astrophysical origin, the need for accurate intensity measurements becomes evident. This may be seen by the dependence of $I_{v'v''}$ upon $N_{v'}$ in equation [1],

$$[1] \qquad I_{v'v''} = DN_{v'}E^4_{v'v''}\left|\int \psi_{v'} R_e(r)\, \psi_{v''}\, dr\right|^2$$

where $I_{v'v''}$ = intensity of (v', v'') band recorded at the spectrometer,
$N_{v'}$ = population of molecules excited to vibrational level v' in the source,
$E_{v'v''}$ = energy separation between v' and v'' levels,
$\psi_{v'}$ = vibrational wave function of the upper vibrational level v',
$\psi_{v''}$ = vibrational wave function of the lower vibrational level v'',
$R_e(r)$ = electronic transition moment,
r = internuclear separation,
D = a constant depending upon geometry of the optical system and the units employed.

$\left|\int \psi_{v'} R_e(r)\, \psi_{v''}\, dr\right|^2$ is the vibrational transition probability of the band concerned, and in order that equation [1] may be used, together with experimental measures of band intensities, to investigate, for example, the vibrational excitation set up in a source, some prior knowledge of the vibrational transition probability must be obtained. The vibrational wave functions are readily accessible (3) for most molecular levels. The transition moment $R_e(r)$, however, presents more severe difficulties as it is a very formidable task to calculate it for each electronic transition of interest. It has been conventional to assume that it is a very slowly varying function of r (5) and thus that for each of the $v' \rightarrow v''$ bands

[1]*Manuscript received April 2, 1954.*
Contribution from the Department of Physics, University of Western Ontario, London, Ont.

$$\int \psi_{v'} R_e(r) \psi_{v''} dr = \bar{R}_e \int \psi_{v'} \psi_{v''} dr,$$

where $\bar{R}_e$ is the average of this slowly varying function over the contributing range of r. Accurately computed values of squares of the overlap integrals $\int \psi_{v'} \psi_{v''} dr$ are available for a number of important band systems (4, 7).

It is of importance therefore to make an experimental investigation into the validity of the assumption of constancy of $R_e(r)$ in order to determine whether the calculated values of $\left|\int \psi_{v'} \psi_{v''} dr\right|^2$ are sufficient knowledge of the vibrational transition probabilities, or whether any allowance for the variation of R_e with r will have to be made. This paper describes such an experimental investigation in which experimental values of $I_{v'v''}$ have been used to obtain relative values of $\left|\int \psi_{v'} R_e(r) \psi_{v''} dr\right|^2$ for bands of the first positive system of N_2 using equation [1]. A comparison between these values and those of the overlap integral squares $\left|\int \psi_{v'} \psi_{v''} dr\right|^2$ shows that, in fact, some allowance for the dependence of R_e upon r will have to be made, and that the simplifying assumption of constancy is too crude in this case. The evaluation of the dependence of R_e upon r is described in the next paper (13).

Until the present work, a set of reliable band-intensities for the first positive system of nitrogen ($B\ ^3\Pi_g \rightarrow A\ ^3\Sigma_u$) has not been available. Some workers (10, 11, 12) have reported peak intensities for a large number of bands while others (1) have made careful measurements of the integrated intensities of the bands in the sequences $\Delta v = 3, 4, 5$ only. In the work to be described here, the relative intensities of 52 bands belonging to the sequences $\Delta v = -3, -2, -1, 0, 1, 2, 3, 4, 5$ ($\lambda\lambda$ 5,350–17,200 Å) have been measured and used for comparison with the overlap integral squares calculated by Jarmain and Nicholls (8).

EXPERIMENTAL

The instrument used in making the intensity measurements was a Perkin-Elmer Model 12-C infrared recording spectrometer. It was equipped with a dense flint prism and a lead sulphide cell. The dispersion of this instrument at the exit slit was approximately 150, 580, and 920 Å/mm. at wavelengths of 6000, 10,000, and 16,000 Å, respectively. The lead sulphide cell was tested for linearity and was only used in the region of intensities where its response was found to be linear. The normal collimating system of the spectrometer was supplemented by a quartz lens in front of the discharge tube, since it occupied a different position from the globar source normally used with the spectrometer.

The spectrum of the first positive system was excited in a water-cooled heavy-current capillary discharge tube of the Pearse-Hunter (6) type, but somewhat larger than the original. The discharge 'capillary' had an internal diameter and length of 1.2 and 75 cm., respectively. This 'capillary' was viewed end-on through a quartz window by the spectrometer.

The discharge was maintained by a direct current generator capable of supplying a maximum current of 1 amp. at 2000 v. The output voltage of the generator was stabilized electronically, and this was necessary in order to maintain the light output from the tube constant for the whole period of

recording the spectrum. After turning the discharge on and adjusting pressure and voltage conditions so as to obtain an almost constant current, the intensity of a typical band (e.g. (0,0)) was recorded during the five-hour warm-up period necessary to establish equilibrium conditions in the tube. A drift in intensity of a few per cent was observed during this time. After this warm-up period, the variation in the deflection shown by the recorder was about $\pm 0.5\%$. It will be noted that this figure includes any variations in the amplifying and recording system as well as any fluctuations in the intensity output of the tube. It was under these last conditions that the spectrum was recorded, with no further adjustment of tube conditions (1220 v., 0.9 amp., 1.25 mm. of Hg). These conditions were found to be optimum for intense radiation of the first positive system.

The prepurified nitrogen used in these experiments was obtained from the Mattheson Company, New Jersey, and was pumped continuously through the tube. The recording of the spectrum was interrupted at a number of wavelengths to ascertain that the intensity of the (0,0) band, which was used as an 'internal monitor' of intensity variations, had not fluctuated during the recording. The slit width used was 0.013 mm. except for the very weak sequence $\Delta v = 5$ ($\lambda\lambda$ 5370–5630 Å) for which the slit width was increased to 0.025 mm.

Intensity calibration measurements of the optical system and detector combined were made by recording the spectrum of a General Electric standard lamp with tungsten filament and quartz window, placed so that the center of its filament was at the position previously occupied by the near end of the discharge capillary. This lamp had been calibrated by the makers. The spectrum of a mercury arc placed in the same position was also recorded in order to provide data for wavelength calibration and dispersion correction for the standard lamp spectrum. The data obtained from these two spectra were used together with the tabulated values of the emissivity of tungsten interpolated from the results collected by Forsythe and Adams (2) to give values of the relative efficiency of the whole optical system at approximately 257 Å intervals corresponding to the wavelengths at which the radiation function was tabulated (9). Values of the relative efficiency versus wavelength were plotted on a large graph, and the relative efficiency for any wavelength could be read from a smooth curve which was drawn through the plotted points. It was noted that there was practically no scatter in the values of the relative efficiency. However, this was only a partial indication of the accuracy with which the values had been determined. The complete curve would have been tilted if the temperature used in determining the values of Planck's radiation function were not the true temperature of the lamp filament. It was found that the ratio of radiant energy per unit wavelength interval at 5400 Å to that at 17200 Å (approximate range of intensity measurements) would be in error by approximately 0.4% for each degree the temperature might have been in error. The precision of the manufacturer's calibration of the standard lamp is not known but it is expected that it is not in error by more than a few degrees.

REDUCTION OF DATA

The profiles of the bands observed were not ideal for immediate interpretation in terms of relative intensities because of the complicated blended rotational structure of each band, and also because of the partial overlap of bands caused both by development of rotational structure and by the dispersion of the spectrometer employed. The following procedure of 'synthetic' separation of the band areas was therefore employed.

For most bands, the sharply falling leading edge of each band was continued as a straight line down to zero intensity and the shape of the tail of the adjacent band was then found by a subtraction of ordinates. For a few weak bands each of which appeared blended on the tail of a very strong band, it was necessary to reverse the procedure and to continue the tail of the strong band down to zero intensity and to subtract ordinates. Although this procedure is open to some criticism, it is the simplest objective one which can be used when the bands are not completely separated. The area under each band so separated was measured with a polar planimeter and then corrected for the relative efficiency of the system from the calibration curve described above. The relative intensities obtained in this way are shown in Table I scaled to (0,0) = 1000.

TABLE I

RELATIVE INTENSITIES OF THE BANDS OF THE FIRST POSITIVE SYSTEM

v' \ v''	0	1	2	3	4	5	6	7	8
0	1000	434	154						
1	1260		261	171	98.1				
2	719	862	214	102	126	81.4			
3	142	833	305	271	102	96.9	100		
4		335	872	94.7	252				
5		73.1	504	590		180			
6		12.6	111	548	362	134			
7			16.8	154	506	161	166		
8				29.3	193	408			
9					39.2	218	318		
10						41.1	210	211	
11							45.5	210	131
12								52.4	170

INTERPRETATION OF RESULTS

From equation [1] the 'vibrational transition probability' may be written:

[2] $$p_{v'v''} = I_{v'v''}\lambda^4_{v'v''}/GN_{v'}$$

where G is a constant depending upon the geometry of the system and upon the units employed, and $\lambda_{v'v''}$ is the wavelength corresponding to the center of the band at half intensity. Although it is usual in a calculation of this sort to use the wavelength of the band head, the center of the band at half intensity seemed to be a more reasonable objective choice here in view of the fact that the bands do not exhibit marked heads and band shape changes from band to band.

The wavelengths which were used are shown in Table II, and Table III lists the values of $p_{v'v''}N_{v'}$ ($\propto I_{v'v''}\lambda^4_{v'v''}$) scaled to $p_{00}N_0 = 1000$. It will be noticed that since the values for each v''-progression (v' = const.) still contain $N_{v'}$, a

TABLE II

WAVELENGTHS OF THE BANDS OF THE FIRST POSITIVE SYSTEM IN Å

v' \ v''	0	1	2	3	4	5	6	7	8
0	10,387	12,211	14,735						
1	8,851		11,800	14,043	17,192				
2	7,694	8,673	9,850	11,436	13,420	16,163			
3	6,824	7,569	8,504	9,594	11,110	12,844	15,370		
4		6,741	7,451	8,315	9,368				
5		6,098	6,661	7,338		9,147			
6		5,571	6,039	6,583	7,229	7,981			
7			5,533	5,985	6,505	7,121	7,831		
8				5,496	5,931	6,432			
9					5,459	5,879	6,360		
10						5,424	5,829	6,291	
11							5,390	5,779	6,221
12								5,352	5,730

TABLE III

$p_{v'v''}N_{v'}$ FOR FIRST POSITIVE SYSTEM

v' \ v''	0	1	2	3	4	5	6	7	8
0	1000	828	625						
1	663		434	570	736				
2	216	419	173	150	351	477			
3	26.4	235	137	197	133	227	479		
4		59.4	231	38.9	167				
5		8.69	85.2	147		108			
6		1.05	12.6	88.5	84.9	46.6			
7			1.35	17.0	77.8	35.6	53.7		
8				2.30	20.5	60.0			
9					2.99	22.4	44.8		
10						3.05	20.9	28.4	
11							3.30	20.2	16.8
12								3.70	15.8

comparison between transition probabilities from theory and experiment can only be made along a v''-progression, for each band of which $N_{v'}$ will be the same.

For each v''-progression, the values of $p_{v'v''}N_{v'}$ given in Table III have been rescaled and are compared in Table IV with the theoretical squares of overlap integrals previously referred to (8). For ease in comparison, the scaling has been such that entries of both theoretical and experimental data for the first band of each progression are equal.

In order to allow comparison to be easily made between these two sets of data, they are presented in block diagram form in Fig. 1. It will be noted from this diagram that while there is some agreement between the relative sizes of the experimental and theoretical values of the transition probabilities for

TABLE IV

COMPARISON OF THEORETICAL AND EXPERIMENTAL TRANSITION PROBABILITIES FOR BANDS OF THE FIRST POSITIVE SYSTEM

v' \ v''	0	1	2	3	4	5	6	7	8	9	10	11	12
0	.340 (.340)	.323 (.282)	.190 (.213)	.088	.014	.005	.002						
1	.406 (.406)	.002	.103 (.266)	.177 (.349)	.148 (.451)	.089	.042	.018	.009	.004	.002		
2	.200 (.200)	.212 (.388)	.113 (.160)	.002 (.139)	.074 (.325)	.126 (.442)	.119	.078	.043	.021	.008	.005	.002
3	.050 (.050)	.301 (.445)	.039 (.259)	.161 (.373)	.031 (.252)	.009 (.430)	.069 (.907)	.097	.089	.076	.041	.021	.012
4	.006	.134 (.134)	.273 (.521)	.001 (.088)	.113 (.377)	.086	.004	.018	.063	.084	.080	.055	.036
5		.027 (.027)	.210 (.265)	.184 (.457)	.046	.044 (.336)	.104	.037	.000	.023	.057	.073	.063
6		.003 (.003)	.059 (.036)	.259 (.253)	.083 (.243)	.107 (.133)	.003	.084	.074	.014	.002	.028	.051
7			.008 (.008)	.103 (.101)	.269 (.461)	.020 (.211)	.128 (.318)	.006	.040	.076	.036	.003	.006
8				.018 (.018)	.161 (.160)	.240 (.470)	.000	.118	.035	.010	.068	.061	.017
9				.002	.035 (.035)	.201 (.262)	.188 (.525)	.016	.077	.068	.000	.033	.063
10					.004	.054 (.054)	.228 (.370)	.130 (.503)	.055	.037	.081	.014	.008
11						.004	.086 (.086)	.273 (.526)	.060 (.438)	.080	.010	.073	.030
12							.012	.116 (.116)	.267 (.495)	.030	.107	.000	.056

NOTE: *The experimental values are given in parentheses scaled such that the value for the first band of each v''-progression is equal to the theoretical value for the same band.*

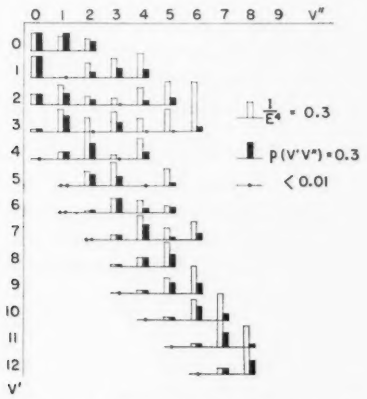

FIG. 1. Comparison of theoretical and experimental transition probabilities for the first positive system.

neighboring bands in a v''-progression, nevertheless the experimental and theoretical values tend to diverge along the progression. Passing out along a progression to higher quantum numbers entails the use of an increasingly greater range of r in $\int \psi_{v'} R_e(r) \psi_{v''} dr$. This divergence between $\left|\int \psi_{v'} R_e(r) \psi_{v''} dr\right|^2$ and $\left|\int \psi_{v'} \psi_{v''} dr\right|^2$ noticed for increasing range of integration in r suggests that the simple assumption of $R_e(r)$ being sensibly independent of r is not justified.

The data presented here will be used in the following paper to find the dependence of the electronic transition moment on internuclear separation.

The research reported in this paper has been sponsored by the Air Force Cambridge Research Centre under Contract AF-19(122)-470.

REFERENCES

1. ELLIOTT, A. and CAMERON, W. H. B. Proc. Phys. Soc. (London), 46: 801. 1934.
2. FORSYTHE, W. E. and ADAMS, E. Q. J. Opt. Soc. Amer. 35: 108. 1945.
3. FRASER, P. A. and JARMAIN, W. R. Private communication.
4. FRASER, P. A., JARMAIN, W. R., and NICHOLLS, R. W. Astrophys. J. 119: 286. 1954.
5. HERZBERG, G. Spectra of diatomic molecules, 2nd ed. D. Van Nostrand Company Inc., New York. 1950. p. 200.
6. HUNTER, A. and PEARSE, R. W. B. J. Sci. Instr. 13: 403. 1936.
7. JARMAIN, W. R., FRASER, P. A., and NICHOLLS, R. W. Astrophys. J. 118: 228. 1953.
8. JARMAIN, W. R. and NICHOLLS, R. W. Can. J. Phys. 32: 201. 1954.
9. LOWAN, A. N. and BLANCH, G. J. Opt. Soc. Amer. 30: 70. 1940.
10. PEARSE, R. W. B. and GAYDON, A. G. The identification of molecular spectra. 2nd ed. Chapman and Hall, Limited, London. 1950.
11. POETKER, A. H. Phys. Rev. 30: 812. 1927.
12. TAWDE, N. R. and PATANKAR, V. S. Phil. Mag. (Ser. 7), 38: 65. 1947.
13. TURNER, R. G. and NICHOLLS, R. W. Can. J. Phys. 32: 475. 1954.

AN EXPERIMENTAL STUDY OF BAND INTENSITIES IN THE FIRST POSITIVE SYSTEM OF N_2

II. THE TRANSITION MOMENT[1]

By R. G. Turner and R. W. Nicholls

ABSTRACT

Experimental band intensities of the first positive system ($B\ ^3\Pi_g \longrightarrow A\ ^3\Sigma_u$) of nitrogen are used together with theoretical transition probabilities to determine the dependence of the electronic transition moment on the internuclear separation. Over the range $1.17 < r < 1.59$ Å of internuclear separation, this dependence may be represented by $R_e(r) = \text{const.} \times \exp(-3.02\, r)$.

INTRODUCTION

In part I, hereafter referred to as I (3), a measure of agreement was reported between the relative magnitudes of theoretical (overlaps squared) and experimental vibrational transition probabilities for neighboring bands in a v''-progression. However, there was a decided trend of experimental values away from the theoretical values along a v''-progression. This divergence suggested the invalidity of the conventional simplifying assumption made in computing the vibrational transition probabilities, namely that the electronic transition moment $R_e(r)$ for the system was roughly independent of internuclear separation r. On this assumption, the vibrational transition probabilities had been computed as the squares of the overlap integrals of the corresponding wave functions (2), i.e., $p(v', v'') = \left|\int \psi_{v'}\, \psi_{v''}\, dr\right|^2$.

In this present paper, experimental intensities and the theoretical overlap integrals are used conjointly to obtain the dependence of $R_e(r)$ on r for the first positive system of N_2. Such information is very difficult to obtain by theoretical means, since it would require detailed knowledge of the electronic wave functions of the states involved. With a knowledge of the dependence of $R_e(r)$ on r, the previous overlap squares may be modified to give an array which represents more closely the values of the vibrational transition probabilities. These are indicative of the distribution of the 'oscillator strength' of the electronic transition through the bands of the system.

METHOD AND RESULTS

The method used here for determining the form of the electronic transition moment has been suggested and fully described by Fraser (1). He shows that the following may be written for the ratio of the values of the electronic transition moment for any two bands in a v''-progression:

$$[1] \qquad \frac{R_e(\bar{r}_{v'v''})}{R_e(\bar{r}_{v'n})} = \frac{\lambda^2_{v'v''} I^{\frac{1}{2}}_{v'v''}}{(v', v'')} \Big/ \frac{\lambda^2_{v'n} I^{\frac{1}{2}}_{v'n}}{(v', n)}.$$

In equation [1] $\lambda_{v'v''}$ and $\lambda_{v'n}$ are characteristic wavelengths for the respective bands while $I_{v'v''}$ and $I_{v'n}$ are respectively the integrated intensities of the

[1]*Manuscript received April 2, 1954.*
Contribution from the Department of Physics, University of Western Ontario, London, Ont.

same bands. The subscript n refers to one particular band in a v''-progression. $\bar{r}_{v'v''}$, which is a kind of average internuclear separation for the $v' \rightarrow v''$ transition, is defined by:

$$\bar{r}_{v'v''} = \frac{(v', r, v'')}{(v', v'')} \qquad [2]$$

where

$$(v', v'') = \int \psi_{v'} \psi_{v''} \, dr,$$

$$(v', r, v'') = \int \psi_{v'} r \psi_{v''} \, dr.$$

Equation [1] enables an experimental determination to be made of the variation of the ratio $R_e(r)/R_e(\bar{r}_{v'n})$ along a v''-progression using the experimental results of I and the previously reported theoretical values of (v', v'') (2). These ratios for each observed v''-progression of the system are shown in Table I.

TABLE I

$R_e(\bar{r}_{v'v''})/R_e(\bar{r}_{v'n})$ FOR BANDS OF THE FIRST POSITIVE SYSTEM
(the scale is different for each v''-progression)

v' \ v''	0	1	2	3	4	5	6	7
0	1.00	0.933	1.06					
1	1.00		1.61	1.41	1.74			
2	1.00	1.35	1.19	10.3*	2.09	1.86		
3	1.00	1.22	2.60*	1.53	2.87*	6.81*		
4		1.00	1.38	8.27*	1.83			
5		1.00	1.12	1.58		2.79*		
6		1.04	1.00	1.26	2.19*	1.45		
7			1.01	1.00	1.33	3.29*	1.60	
8				1.02	1.00	1.40		
9					0.854	1.00	1.46	
10						0.787	1.00	1.54

In order to interpret the variation as a function of r, the value of $\bar{r}$ appropriate to each band of the system must be found. The $\bar{r}_{v'v''}$ were calculated by the simple method suggested by Jarmain (1) rather than through the definition of $\bar{r}_{v'v''}$ in equation [1]. The $\bar{r}$ for a large number of bands are given in Table II, and thus a value of $\bar{r}$ may be associated with each ratio $R_e(\bar{r}_{v'v''})/R_e(\bar{r}_{v'n})$.

TABLE II

$\bar{r}$ IN Å FOR BANDS OF THE FIRST POSITIVE SYSTEM

v' \ v''	0	1	2	3	4	5	6	7	8	9	10	11	12
0	1.255	1.222	1.193										
1	1.297	1.261	1.228	1.200	1.173								
2	1.346	1.304	1.268	1.235	1.206	1.180							
3	1.403	1.353	1.311	1.275	1.242	1.213	1.187						
4	1.469	1.410	1.360	1.318	1.281	1.249	1.220	1.194					
5	1.552	1.476	1.417	1.367	1.324	1.288	1.256	1.227	1.201	1.177			
6		1.560	1.484	1.424	1.374	1.332	1.295	1.263	1.234	1.208	1.185		
7			1.568	1.491	1.432	1.382	1.339	1.302	1.270	1.242	1.215	1.191	
8				1.576	1.498	1.439	1.389	1.346	1.309	1.277	1.249	1.223	1.199
9					1.584	1.507	1.446	1.397	1.354	1.317	1.285	1.256	1.230
10						1.592	1.514	1.454	1.404	1.362	1.324	1.293	1.264
11							1.600	1.523	1.462	1.412	1.370	1.332	1.300
12									1.531	1.470	1.420	1.378	1.340

Before discussing how the ratios in Table I are brought to the same scale and thus linked together over the whole range of r covered by the $\bar{r}_{v'v''}$ of the observed bands, brief mention will be made of the reasons for rejecting some of the points which at this stage were considered unreliable. For each v''-progression a graph of $R_e(r)/R_e(\bar{r}_{v'n})$ versus r was plotted, and the data for points which lay far from a smooth curve representative of the trend of the other points were discarded after careful examination. These bands are marked with an asterisk in Table I. The discarded bands had a low overlap integral in all cases, and it was thought that the percentage error in these might be relatively high. Also there may have been some overlapping of the sequences in the spectrum. The resultant overlapping of a band of one sequence with a weak band from another sequence would probably not be noticed in some cases by a change in profile at the low dispersion of the spectrometer used. Thus the intensity taken as due to one band in the sequence $\Delta v = a$ might actually be due both to it and to a weak band far out in the sequence $\Delta v = a - 1$. This would introduce a large error only in the case of weak bands.

The remaining points on each graph of $R_e(r)/R_e(\bar{r}_{v'n})$ versus r were connected by straight lines. The relative values $R_e(\bar{r}_{v'v''})/R_e(\bar{r}_{v'n})$ from two v''-progressions were brought to the same scale by normalizing the areas under the lines in the common interval in r. This process, which is demonstrated in Fig. 1, was used to set the data for all progressions at the same scale as the

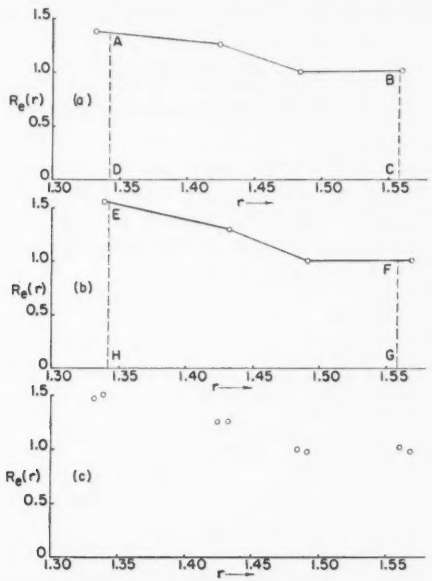

FIG. 1. Scaling procedure for $R_e(\bar{r}_{v'n})/R_e(\bar{r}_{v'v''})$ values:
(*a*) $v' = 6$ progression, (*b*) $v' = 7$ progression, (*c*) $v' = 6$ and $v' = 7$ progressions combined. $R_e(\bar{r}_{v'n})/R_e(\bar{r}_{v'v''})$ values of $v' = 7$ progression have been brought to the same scale as the $v' = 6$ progression by multiplying them by $\dfrac{\text{area } ABCD}{\text{area } EFGH}$.

$v' = 0$ progression. These scaled values of $R_e(\bar{r}_{v'v''})/R_e(\bar{r}_{v'n})$ are given in Table III. They represent the variation of $R_e(r)$ with r for the band system. While the values of $R_e(r)$ at the $\bar{r}_{v'v''}$ in Table III are all expressed on the same scale,

TABLE III

$R_e(\bar{r}_{v'v''})/R_e(\bar{r}_{00})$ FOR BANDS OF THE FIRST POSITIVE SYSTEM

v' \ v''	0	1	2	3	4	5	6	7
0	1.00	0.933	1.06					
1	0.653		1.05	0.920	1.14			
2	0.563	0.760	0.670		1.18	1.05		
3	0.495	0.604		0.757				
4		0.424	0.585		0.776			
5		0.414	0.463	0.653				
6		0.412	0.396	0.499		0.574		
7			0.380	0.376	0.500		0.601	
8				0.373	0.365	0.512		
9					0.311	0.364	0.531	
10						0.277	0.352	0.541

this scale is still arbitrary. Absolute values could be obtained only through theoretical calculations or lifetime measurements.

DISCUSSION

In an attempt to represent the information given in Tables II and III in functional form, the values of $\bar{r}$ were assumed to be exact, and it was found that

$$R_e(r) = \exp(3.61 - 3.02r) \qquad [3]$$

was a good representation of the dependence of R_e on r over the range of r covered by the bands of the system that were used ($1.17\ \text{Å} < r < 1.59\ \text{Å}$). The constants in equation [3] were found from a least squares analysis of $\log R_e(r)$ versus r. Because of the arbitrary scale of $R_e(r)$ no significance can be attached to the constant factor in equation [3]. The curve and the data which it represents are shown in Fig. 2. Following standard procedure, the probable error in the ratio of two $R_e(r)$ values is

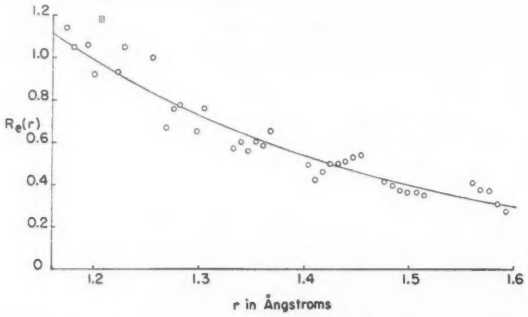

FIG. 2. $R_e(r)$ versus r for the first positive system of nitrogen.

$$[4] \qquad P(r_1, r_2) = \pm 0.10(r_1 - r_2) \exp -3.02(r_1 - r_2).$$

Using equations [3] and [4], the following values and limits are obtained:

$$\frac{R_e(1.17)}{R_e(1.38)} = 1.89 \pm 0.04, \qquad \frac{R_e(1.17)}{R_e(1.59)} = 3.56 \pm 0.15.$$

It will be noted that these limits have been determined by the scatter of the data. However, as was pointed out in I, any inaccuracy in the manufacturer's calibration of the standard lamp used in the work would further widen the ranges of error given above.

Thus an expression has been found to represent the shape of the electronic transition moment for the first positive system of nitrogen. This may be used in calculating more accurate values of vibrational transition probabilities. However, it must be noted that it can only be used for bands whose $\bar{r}$ falls in the range covered by the values used in determining equation [3], i.e., $1.17 \text{ Å} < r < 1.59 \text{ Å}$.

ACKNOWLEDGMENTS

The authors wish to express their sincere thanks to Drs. R. C. Dearle and P. A. Fraser and also to Mr. W. R. Jarmain for many helpful discussions on various aspects of this work. The research reported in this paper has been sponsored by the Air Force Cambridge Research Center under Contract AF 19(122)-470.

REFERENCES

1. FRASER, P. A. Can. J. Phys. In press, 1954.
2. JARMAIN, W. R. and NICHOLLS, R. W. Can. J. Phys. 32: 201. 1954.
3. TURNER, R. G. and NICHOLLS, R. W. Can. J. Phys. 32: 468. 1954.

DESCRIPTION OF A COMPOSITE PARTICLE IN TERMS OF A FUNCTIONAL POTENTIAL WELL[1]

By R. Finkelstein, S. G. Gasiorowicz,[2] and P. Kaus

ABSTRACT

A covariant two-particle wave equation of the following form is investigated:

$$[D_1 + D_2 + gF(\psi)]\,\Psi = 0$$

where D_k is the Dirac operator $(\gamma_\mu p_\mu - im)_k$ and $F(\psi)$ is a functional "potential well". $\Psi_{\alpha\alpha}$ is interpreted as a probability amplitude and transforms as a spinor on both indices. ψ is the internal wave function depending only on the relative coordinates. This equation provides a covariant model which exhibits nonlocal interactions and can be studied by relatively simple methods. The investigation is primarily methodological. The physical model is similar to the Fermi–Yang pion and like it, is qualitative and not based on fundamental theory.

INTRODUCTION

It has been suggested by Fermi and Yang (6) that the pion consists of a nucleon bound to an antinucleon.* Since such a model does not fit very well into the framework of current field theory, any elaborate investigation in terms of this theory would probably not be promising; but of course in other theories the situation may be different. In this paper such an alternative theory is *not* considered, and the existence of the composite pion is simply assumed without any attempt at justification in terms of fundamental theory. One conceivable structure is then investigated by means of a formally simple wave equation which is covariant and has for bound state problems approximately the same physical content as the Fermi–Yang picture.

This equation is

$$[D_1 + D_2 + gF(\psi)]\Psi = 0 \qquad [1]$$

where $D_k = \gamma_\mu^{(k)}\, p_\mu^{(k)} - im^{(k)}$ is a Dirac operator.

$\Psi_{\alpha\alpha}(x^{(1)}, x^{(2)})$, to be interpreted as a probability amplitude, is a function of the eight space–time coordinates and transforms as a spinor on both indices; ψ depends only on $x_\mu^{(1)} - x_\mu^{(2)}$. $F(\psi)$ is an invariant functional of ψ; it is responsible for the interaction between the two particles and formally resembles a potential well. In order to give a simple discussion Fermi and Yang assumed a square well interaction; equation [1] may be regarded as having been obtained from their picture by replacement of the Dirac hamiltonian plus a square well by a covariant operator.

[1] *Manuscript received April 9, 1954.*
Contribution from the University of California at Los Angeles.
The preparation of this paper was sponsored (in part) by the Office of Naval Research, United States Navy, while one of us (S. G.) was at the Institute for Numerical Analysis, National Bureau of Standards.

[2] *Now at the Radiation Laboratory, Berkeley, California.*

**There were earlier suggestions of the same nature by de Broglie (2) and Rosen (11). The work reported here was finished at about the same time as three other studies of the same model: de Broglie and Tonnelat (4); de Broglie (3); and Moseley and Rosen (10). At the present time the combination D_1D_2 in equation [1] would appear more interesting than $D_1 + D_2$, but the same method may be used in the two cases. Unfortunately the multiplicative combination has not been studied.*

F is chosen to be a simple invariant which becomes important when the two particles are close ($\sim\hbar/Mc$). For example if $F = \psi^+\psi$ and ψ has the range $\hbar/Mc$, then the effective potential well will have a comparable but somewhat smaller range. The constant g has the dimensions of a Fermi constant and in the pion problem is of the order $(Mc^2)(\hbar/Mc)^3 \cong 10^{-45}$ erg cm^3.

Although [1] is covariant, it may deviate from relativity, since $F(\psi)$—depending on its form—may permit interactions outside of the light cone; thus equation [1] is general enough to exhibit nonlocal interactions. This action-at-a-distance goes beyond the correlations already present in quantal descriptions (5),* especially if F does not depend explicitly on coordinate separation. In the following, since we shall be concerned only with bound state problems, we may ignore any explicit dependence of F on coordinate separation without getting unphysical results.

TRANSFORMATION PROPERTIES

We require that $\Phi_{a\alpha}(x_\mu^{(1)}, x_\mu^{(2)})$ transform like the probability amplitude for annihilation of a negative meson, i.e., like $[N_>(x_\mu^{(1)})]_a\,[P_<{}^*(x_\mu^{(2)})]_\alpha$ where $N_>$ and $P_<$ denote spinors belonging to a positive energy neutron and negative energy proton respectively. Let $\Psi = \Phi C^{-1}$ where C is a charge conjugation operator; then Ψ transforms like $(N_>)_a(\bar{P}_>)_\alpha$ where $\bar{P}_>$ is the wave function of a positive energy antiproton. We characterize the (negative) pion by Ψ or Φ.

Under the Lorentz rotation (S)

$$[2a] \qquad (\Phi\gamma_4)' = S(\Phi\gamma_4)\,S^{-1},$$

$$[2b] \qquad (\Psi T)' = S(\Psi T)\,S^{-1}$$

where $T = -iC\gamma_4$, $T\gamma_\mu T^{-1} = -\tilde{\gamma}_\mu$, and $\sim$ denotes transposition.

Under space inversion

$$[3a] \qquad (\Phi\gamma_4)' = \epsilon_{N_>}\epsilon^*_{P_<}\gamma_4(\Phi\gamma_4)\,\gamma_4,$$

$$[3b] \qquad (\Psi T)' = \epsilon_{N_>}\epsilon^*_{P_<}\gamma_4(\Psi T)\,\gamma_4$$

where $\epsilon_{N_>}$, for example, is ± 1 depending upon inversion properties assigned to $N_>$. Take both P and N of type A (Yang and Tiomno (12)) so that

$$[4] \qquad \epsilon_{N_>}\epsilon^*_{P_<} = -1.$$

Now expand $\Phi\gamma_4 = i\Psi T$ in a complete set of 16 independent matrices as follows:

$$[5] \qquad \Gamma^0_0 = 1, \quad \Gamma^1_\mu = \epsilon^\alpha_\mu\gamma_\alpha, \quad \Gamma^2_{\mu\nu} = \frac{1}{2!}\epsilon^{\alpha\beta}_{\mu\nu}\gamma_\alpha\gamma_\beta,$$

$$\Gamma^3_{\mu\nu\sigma} = \frac{1}{3!}\epsilon^{\alpha\beta\gamma}_{\mu\nu\sigma}\gamma_\alpha\gamma_\beta\gamma_\gamma, \quad \Gamma^4_{\mu\nu\sigma\tau} = \frac{1}{4!}\epsilon^{\alpha\beta\gamma\delta}_{\mu\nu\sigma\tau}\gamma_\alpha\gamma_\beta\gamma_\gamma\gamma_\delta$$

**It is clear that equation [1] is not a proper quantal equation since the probability amplitude does not even satisfy a linear equation. There is some formal resemblance between the model studied here and the work of Bohm (1) in that the wave function plays a dual role, being responsible for forces as well as for probabilities; but the similarity stops here.*

where $\epsilon_{b_1 \ldots b_n}^{a_1 \ldots a_n}$ is totally antisymmetric and of absolute value unity.

Write

$$\Phi\gamma_4 = i\Psi T = \sum_{\sigma,\rho} \Lambda_\rho^\sigma(x_\mu^{(1)}, x_\mu^{(2)})\, \Gamma_\rho^\sigma \tag{6}$$

where ρ stands for all the σ subscripts of Γ^σ.

Under the Lorentz rotation

$$(\Phi\gamma_4)' = (i\Psi T)' = \sum \Lambda_{\rho'}^{\sigma'}\Gamma_{\rho'}^{\sigma'}, \tag{7a}$$

$$S^{-1}\Gamma_\rho^\sigma S = \sum a_{\rho\rho'}^{\sigma\sigma'}\Gamma_{\rho'}^{\sigma'}, \tag{7b}$$

$$\Lambda_{\rho'}^{\sigma'} = \sum a_{\rho'\rho}^{\sigma'\sigma}\Lambda_\rho^\sigma. \tag{7c}$$

Since we have taken $\epsilon_{N_>}\epsilon_{P_<}^* = -1$, it follows from [7c] that Λ_ρ^σ is the ρ-component of a tensor of rank† $(4 - \sigma)$.

The treatment of the adjoint functions Φ^+ and Ψ^+ (transforming like $(N_>)^+(P_<^*)^+$ and $(N_>)^+(\bar{P}_>)^+$ respectively) follows similarly from the definitions

$$\Phi^+ = -\bar{\gamma}_4\, \Phi^*\gamma_4, \tag{8a}$$

$$\Psi^+ = -\bar{\gamma}_4\, \Psi^*\gamma_4. \tag{8b}$$

THE EQUATIONS OF MOTION

The equations of motion may be derived from the Lagrangian

$$\mathscr{L} = \int\int L\, d_4x^{(1)} d_4x^{(2)} \tag{9}$$

where

$$L = L_0 + L_1 + L_2, \tag{9a}$$

$$L_0 = (\tfrac{1}{2})[\Psi_{\alpha a}^+\{\gamma_\mu^{(1)} p_\mu^{(1)} + \gamma_\mu^{(2)} p_\mu^{(2)}\}_{\alpha a,\beta b}\Psi_{\beta b} - \{(p_\mu^{(1)}\Psi^+)_{\alpha a}(\gamma_\mu^{(1)})_{\alpha a,\beta b} + (p_\mu^{(2)}\Psi^+)_{\alpha a}(\gamma_\mu^{(2)})_{\alpha a,\beta b}\}\Psi_{\beta b}], \tag{9b}$$

$$L_1 = -2iM\Psi_{\alpha a}^+\Psi_{\alpha a}, \tag{9c}$$

and L_2 is the interaction term. In terms of Λ_ρ^σ this Lagrangian is

$$L_0 = (\tfrac{1}{2})(-)^{\sigma - s_4'}\mathrm{Tr}[\Gamma_{\rho'}^{\sigma'+}\gamma_\mu\Gamma_\rho^\sigma(\Lambda_{\rho'}^{\sigma'*} p_\mu^{(1)}\Lambda_\rho^\sigma - \Lambda_\rho^\sigma p_\mu^{(1)}\Lambda_{\rho'}^{\sigma'*}) - (\Gamma_{\rho'}^{\sigma'+}\Gamma_\rho^\sigma\gamma_\mu)(\Lambda_{\rho'}^{\sigma'*} p_\mu^{(2)}\Lambda_\rho^\sigma - \Lambda_\rho^\sigma p_\mu^{(2)}\Lambda_{\rho'}^{\sigma'*})], \tag{10a}$$

$$L_1 = -8iM(-)^{\sigma' - s_4'}\Lambda_{\rho'}^{\sigma'*}\Lambda_{\rho'}^{\sigma'} \tag{10b}$$

where s_4 is the number of times γ_4 appears in Γ_ρ^σ, thus

$$\Gamma_\rho^\sigma = \pm\, \gamma_1^{s_1} \ldots \gamma_4^{s_4}.$$

†*If P and N had been assigned opposite type* ($\epsilon_{N_>}\epsilon_{P_<}^* = 1$) Λ_ρ^σ *would have been the* ρ*-component of a tensor of rank* σ.

The equations of motion

$$[11a] \qquad p_\mu^{(1)}[\partial L/\partial(p_\mu^{(1)}\Lambda_{\rho'}^{\sigma'*})] + p_\mu^{(2)}[\partial L/\partial(p_\mu^{(2)}\Lambda_{\rho'}^{\sigma'*})] = (\partial L/\partial\Lambda_{\rho'}^{\sigma'*})$$

become

$$[11b] \quad \mathrm{Tr}(\Gamma_{\rho'}^{\sigma'+}\gamma_\mu\Gamma_\rho^\sigma)p_\mu^{(1)}\Lambda_\rho^\sigma - \mathrm{Tr}(\Gamma_{\rho'}^{\sigma'+}\Gamma_\rho^\sigma\gamma_\mu)p_\mu^{(2)}\Lambda_\rho^\sigma - 8iM\Lambda_{\rho'}^{\sigma'} + (-)^{\sigma'+s_{\sigma'}}(\partial L_2/\partial\Lambda_{\rho'}^{\sigma'*}) = 0.$$

The composite system is separated into an "internal" and an "external" one by the usual transformation

$$[12] \qquad P_\mu^{\mathrm{op}} = p_\mu^{(1)} + p_\mu^{(2)}, \qquad p_\mu^{\mathrm{op}} = (\tfrac{1}{2})(p_\mu^{(1)} - p_\mu^{(2)}),$$
$$X_\mu = (\tfrac{1}{2})(x_\mu^{(1)} + x_\mu^{(2)}), \qquad x_\mu = x_\mu^{(1)} - x_\mu^{(2)}$$

where P_μ^{op} (p_μ^{op}) are the external (internal) momentum operators; X_μ and x_μ are the corresponding position coordinates. In the case of the *free* pion one may further write

$$[13] \qquad \Lambda_\rho^\sigma(x_\mu^{(1)}, x_\mu^{(2)}) = \frac{1}{(\Omega)^{\frac{1}{2}}}\lambda_\rho^\sigma(x_\mu)\, e^{iP_\mu X_\mu},$$

$$[14] \qquad P_\mu^{\mathrm{op}}\, e^{\pm iP_\mu X_\mu} = \pm P_\mu\, e^{\pm iP_\mu X_\mu}$$

and the equations of motion become

$$[15] \quad {}^{+}_{\mu}A^{\sigma\sigma'}_{\rho\rho'}p_\mu\lambda_\rho^\sigma + \tfrac{1}{2}\,{}^{-}_{\mu}A^{\sigma\sigma'}_{\rho\rho'}P_\mu\lambda_\rho^\sigma - 8iM\lambda_{\rho'}^{\sigma'} + (-)^{\sigma'+s_{\sigma'}}\Omega^{\frac{1}{2}}(\partial L_2/\partial\lambda_{\rho'}^{\sigma'*}) = 0$$

where

$$[15a] \qquad {}^{\pm}_{\mu}A^{\sigma\sigma'}_{\rho\rho'} = \mathrm{Tr}(\Gamma_{\rho'}^{\sigma'+}\gamma_\mu\Gamma_\rho^\sigma \pm \Gamma_{\rho'}^{\sigma'+}\Gamma_\rho^\sigma\gamma_\mu),$$
$${}^{\pm}_{\mu}A^{\sigma\sigma'}_{\rho\rho'} = 4\epsilon^{\mu\rho_1\ldots\rho_\sigma}_{\rho_1'\ldots\rho'\sigma+1}(1 \pm (-)^\sigma) \quad \text{for } \sigma' = \sigma + 1,$$
$$= 4\epsilon^{\mu\rho_1'\ldots\rho'\sigma-1}_{\rho_1\ldots\rho_\sigma}(1 \pm (-)^{\sigma-1}) \quad \text{for } \sigma' = \sigma - 1.$$

It will now be explicitly assumed that the interaction depends only on the internal wave function, ψ; therefore one may put $\Omega = 1$. The equations of motion can then be written in the following form:

$$[16] \quad \begin{aligned}
&\epsilon_\mu^\alpha p_\mu\lambda_\alpha^1 - iM\lambda_0^0 + (\tfrac{1}{8})\partial L_2/\partial\lambda_0^{0*} = 0,\\
&\epsilon_{\alpha'}^\mu p_\mu\lambda_0^0 - (\tfrac{1}{2})\epsilon_{\mu\alpha'}^{\alpha\beta}P_\mu\lambda_{\alpha\beta}^2 - iM\lambda_{\alpha'}^1 + (-)^{1+s_{\alpha'}}(\tfrac{1}{8})\partial L_2/\partial\lambda_{\alpha'}^{1*} = 0,\\
&\epsilon_{\mu\alpha'\beta'}^{\alpha\beta\gamma}p_\mu\lambda_{\alpha\beta\gamma}^3 + (\tfrac{1}{2})\epsilon_{\alpha'\beta'}^{\mu\alpha}P_\mu\lambda_\alpha^1 - iM\lambda_{\alpha'\beta'}^2 + (-)^{s_{\alpha'}}(\tfrac{1}{8})\partial L_2/\partial\lambda_{\alpha'\beta'}^{2*} = 0,\\
&\epsilon_{\alpha'\beta'\gamma'}^{\mu\alpha\beta}p_\mu\lambda_{\alpha\beta}^2 + (\tfrac{1}{2})\epsilon_{\alpha\beta\gamma\delta}^{\mu\alpha'\beta'\gamma'}P_\mu\lambda_{\alpha\beta\gamma\delta}^4 - iM\lambda_{\alpha'\beta'\gamma'}^3 + (-)^{1+s_{\alpha'}}(\tfrac{1}{8})\partial L_2/\partial\lambda_{\alpha'\beta'\gamma'}^{3*} = 0,\\
&\tfrac{1}{2}\epsilon_{\alpha'\beta'\gamma'\delta'}^{\mu\alpha\beta\gamma}P_\mu\lambda_{\alpha\beta\gamma}^3 - iM\lambda_{\alpha'\beta'\gamma'\delta'}^4 - (\tfrac{1}{8})\partial L_2/\partial\lambda_{\alpha'\beta'\gamma'\delta'}^{4*} = 0.
\end{aligned}$$

The notation used here does not distinguish between covariant and contravariant components.

SPECIAL SOLUTIONS IN THE PROPER SYSTEM OF THE PION

The probability amplitudes determined by the set [16] depend upon the times of both particles in general. There are, however, special solutions which do not depend upon the relative time $t_2 - t_1$; we have been able to investigate only these special solutions. These solutions may be defined by the covariant condition

$$P_\mu p_\mu \Lambda_\rho^\sigma = 0. \tag{17}$$

In the proper system, for which $\mathbf{P} = 0$, $P_4 = im$, [17] becomes

$$p_4 \Lambda_\rho^\sigma = 0 \tag{18a}$$

so that there is no dependence on the relative time. For these solutions one may write

$$\lambda_\rho^\sigma(\ldots;t) = \lambda_\rho^\sigma(\ldots;0) \tag{18b}$$

where on the right-hand side the times of particle 1 and particle 2 have been set equal.

It may be noted that [17] is satisfied in the limit of no interaction, for then

$$2P_\mu p_\mu = (p_\mu^1 + p_\mu^2)(p_\mu^1 - p_\mu^2) = (p_\mu^1)^2 - (p_\mu^2)^2 = (-M)^2 - (-M)^2 = 0.$$

Although there is no reason to require [17] in general, this condition may be used to further limit the model; that will be the procedure here.

The solutions we have been able to obtain are also characterized by simple angular dependence in the proper frame for the pion, namely: λ_0^0, λ_4^1, λ_{123}^3, λ_{1234}^4 are either spherically symmetric or vanish, while the remaining functions have p-orbital dependence or vanish. Such an angular dependence corresponds to a composite particle with zero spin (which is correct for the physical pion).

These solutions may be written in the following special form:

$$\begin{aligned}
&\lambda_0^0 = A(r), \qquad 2!\lambda_{ij}^2 = H(r)(r_k/r), \qquad 3!\lambda_{ijk}^3 = \lambda_4(r), \\
&\lambda_k^1 = a(r)(r_k/r), \quad 2!\lambda_{i4}^2 = E(r)(r_i/r), \qquad 4!\lambda_{ijkl}^4 = \Lambda(r), \\
&\lambda_4^1 = a_4(r), \qquad 3!\lambda_{ij4}^3 = \lambda(r)(r_k/r).
\end{aligned} \tag{19}$$

The equations of motion in the proper system are then:

$$\begin{aligned}
&a' + 2a/r + MA + (i/8)\,\partial L_2/\partial A^* = 0, \\
&A' + \tfrac{1}{2}mE + Ma - (i/8)\,\partial L_2/\partial a^* = 0, \\
&Ma_4 + (i/8)\,\partial L_2/\partial a_4^* = 0, \\
&\lambda_4' + MH + (i/8)\,\partial L_2/\partial H^* = 0, \\
&\tfrac{1}{2}ma + ME - (i/8)\,\partial L_2/\partial E^* = 0, \\
&M\lambda + (i/8)\,L_2/\partial\lambda^* = 0, \\
&H' + 2H/r + \tfrac{1}{2}m\Lambda + M\lambda_4 - (i/8)\,\partial L_2/\partial\lambda_4^* = 0, \\
&\tfrac{1}{2}m\lambda^4 + M\Lambda - (i/8)\,\partial L_2/\partial\Lambda^* = 0.
\end{aligned} \tag{20}$$

It is possible to take the quantities A, a_4, a, H, λ_4, Λ as real and λ, E as imaginary in the center of mass system. These equations split into two sets involving (a, A, E, λ) and (H, λ_4, Λ), respectively, coupled only through the interaction term, L_2. A simple solution of the complete set is obtained if we put

$$a = E = \lambda = 0, \quad A = a_4 = 0, \tag{21}$$

and solve the remaining equations for H, λ_4, and Λ. One is left with the following set of coupled equations:

$$\begin{aligned} &\lambda_4' + MH + (i/8)\,\partial L_2/\partial H = 0, \\ &H' + (2/r)\,H + (m/2)\,\Lambda + M\lambda_4 - (i/8)\,\partial L_2/\partial \lambda_4 = 0, \\ &\tfrac{1}{2}m\lambda_4 + M\Lambda - (i/8)\,\partial L_2/\partial \Lambda = 0. \end{aligned} \tag{22}$$

THE INTERACTION TERM

For simplicity L_2, the interaction term, was chosen of the following form:

$$L_2 = 8igMI_\sigma^2, \tag{23}$$

$$I_\sigma = \sum_\rho \mathrm{Tr}(\tilde{\bar{\psi}}^+ \Gamma_\rho^\sigma \psi \tilde{\Gamma}_\rho^\sigma). \tag{23a}$$

(When ψ is factorable, I_σ may be written in the familiar form:

$$I_\sigma = \sum_\rho (N_>{}^+ \Gamma_\rho^\sigma N_>)(\bar{P}_>{}^+ \Gamma_\rho^\sigma \bar{P}_>).\ )$$

In the notation introduced for the center of mass system one has

$$\begin{aligned} I_0/4 &= A^2 - a^2 + a_4^2 + H^2 - E^2 + \lambda^2 - \lambda_4^2 - \Lambda^2, \\ I_1/4 &= 4A^2 + 2a^2 - 2a_4^2 + 2\lambda^2 - 2\lambda_4^2 + 4\Lambda^2, \\ I_2/4 &= -6A^2 + 2H^2 - 2E^2 + 6\Lambda^2, \\ I_3/4 &= -4A^2 + 2a^2 - 2a_4^2 + 2\lambda^2 - 2\lambda_4^2 - 4\Lambda^2, \\ I_4/4 &= A^2 + a^2 - a_4^2 + H^2 - E^2 - \lambda^2 + \lambda_4^2 - \Lambda^2, \end{aligned} \tag{24}$$

which will be referred to as "scalar", "vector", ... "pseudoscalar" interactions.

SOLUTION OF THE EIGENVALUE PROBLEM

The structure of the composite particle is determined by the set [22]. Solutions are physically admissible only if they are everywhere regular and quadratically integrable. This condition leads to a relation between the two parameters, g, the coupling constant, and m, the mass of the compound system.

It is convenient first to write [24] in dimensionless form. Put

$$J_\sigma = I_\sigma^2, \ r = x/M, \text{ and } m/2M = \nu.$$

The dimensionless equations are then

$$\frac{d\lambda_4}{dx} + H - g\frac{\partial J_\sigma}{\partial H} = 0, \tag{25a}$$

$$\frac{dH}{dx} + \frac{2}{x}H + \nu\Lambda + \lambda_4 + g\frac{\partial J_\sigma}{\partial \lambda_4} = 0, \tag{25b}$$

$$\nu\lambda_4 + \Lambda + g\frac{\partial J_\sigma}{\partial \Lambda} = 0. \qquad [25c]$$

Eigensolutions exist only for a particular relation between ν and g. The eigenproblem will now be discussed by a method described in more detail elsewhere (8)*. One may begin by letting x correspond to time and by investigating the motion of the representative point in the λ_4,H-plane. (It is not necessary to consider motion in the λ_4,H,Λ-space, since Λ may be eliminated by the use of the algebraic equation [25*c*].) It is then convenient to consider the related "conservative system", obtained by deleting terms which contain x explicitly. This system is

$$\frac{d\lambda_4}{dx} + H - g\frac{\partial J_\sigma}{\partial H} = 0,$$

$$\frac{dH}{dx} + \nu\Lambda + \lambda_4 + g\frac{\partial J_\sigma}{\partial \lambda_4} = 0, \qquad [26]$$

$$\nu\lambda_4 + \Lambda + g\frac{\partial J_\sigma}{\partial \Lambda} = 0.$$

This set has an "integral of the motion", denoted by $\mathfrak{H}$ and given by

$$\mathfrak{H} = \nu\lambda_4\Lambda + \tfrac{1}{2}(\lambda_4^2 + \Lambda^2 - H^2) + g J_\sigma. \qquad [27]$$

For the conservative system [26]

$$d\mathfrak{H}/dx = 0$$

but for the complete set [25]

$$\frac{d\mathfrak{H}}{dx} = \frac{2}{x}H^2 - \frac{2gH}{x}\frac{\partial J_\sigma}{\partial H}. \qquad [28]$$

The representative point for [26] thus moves on the curves $\mathfrak{H}$ = constant, while the corresponding point for [25] crosses these contours—in the direction of larger or smaller values of H depending on the sign of $d\mathfrak{H}/dx$. Note that in order to draw $\mathfrak{H}$-contours in the λ_4,H-plane one must eliminate Λ from [27] by [25*c*]. Note also that in this plane an eigensolution is defined as a curve which starts at $H = 0$ and terminates at the origin without ever going to infinity.

We now consider the *vector* interaction in detail. Take

$$J_1 = (2^{-4} I_1)^2 = (\Lambda^2 - \tfrac{1}{2}\lambda_4^2)^2. \qquad [29]$$

The integral $\mathfrak{H}$, which will be called the contour function, is

$$\mathfrak{H} = \nu\lambda_4\Lambda + \tfrac{1}{2}(\lambda_4^2 + \Lambda^2 - H^2) + g(\Lambda^2 - \tfrac{1}{2}\lambda_4^2)^2 \qquad [30]$$

and

$$d\mathfrak{H}/dx = 2H^2/x. \qquad [30a]$$

**The physical problem there is completely unrelated to this paper.*

Since $d\mathfrak{H}/dx \geqslant 0$ the representative point moves toward higher values of $\mathfrak{H}$ in the phase plane. If $g > 0$, $\mathfrak{H}$ increases as $\lambda_4 \to \infty$ and the representative point moves outward instead of toward the origin; it therefore cannot describe an eigensolution. In fact $g > 0$ corresponds to a repulsive interaction and for a bound state solution we require that $g < 0$. Therefore take $g < 0$ and put

$$F = \sqrt{-g}\,\Lambda,\ G = \sqrt{-g}\,\lambda_4,\ E = \sqrt{-g}\,H.$$

The differential equations [25] then become

[31a] $$\frac{dG}{dx} + E = 0,$$

[31b] $$\frac{dE}{dx} + \frac{2}{x}E + \nu F + G + 2G(F^2 - \tfrac{1}{2}G^2) = 0,$$

[31c] $$\nu G = F - 4F(F^2 - \tfrac{1}{2}G^2) = 0.$$

In addition one has

[32a] $$K = -g\mathfrak{H} = \nu FG + \tfrac{1}{2}(F^2 + G^2 - E^2) - (F^2 - \tfrac{1}{2}G^2)^2,$$

[32b] $$\frac{dK}{dx} = -g\frac{d\mathfrak{H}}{dx} = \frac{2}{x}E^2.$$

F may be eliminated by use of the cubic equation [31c], but of course one must choose the root belonging to an eigensolution. This choice may be made by considering G as a function of $W = F^2 - \frac{1}{2}G^2$. The curve

$$G^2 = [2W(1 - 4W)^2]/[2\nu^2 - (1 - 4W)^2]$$

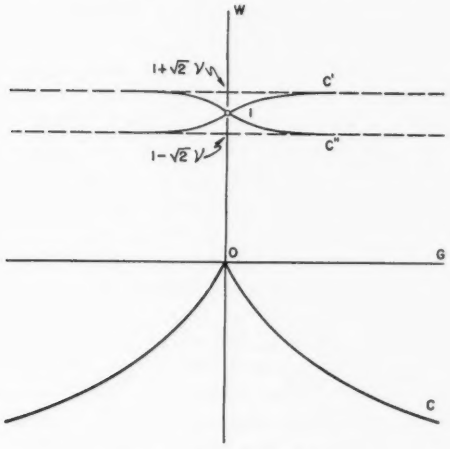

FIG. 1. Plot of G vs. W.

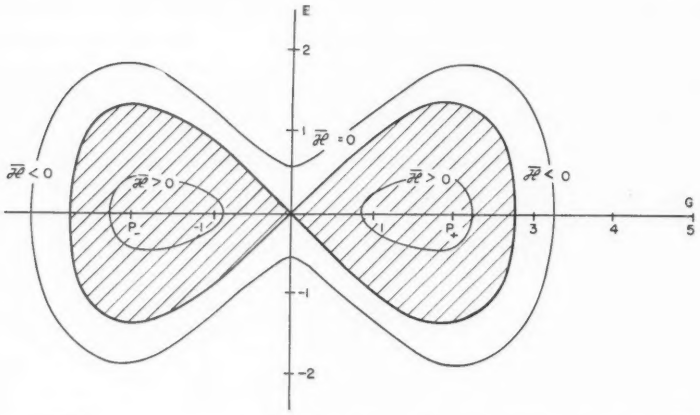

FIG. 2. $\overline{\mathfrak{H}}$ = constant contours in the E,G plane. (Shaded area denotes the region of $\overline{\mathfrak{H}}>0$.)

is shown in Fig. 1, from which one concludes that a solution terminating at the origin (such as an eigensolution) must correspond to the branch $W < 0$. With this information one may then plot the $\mathfrak{H}$ contours in the G–E plane (Fig. 2). It is clear from this figure that a representative point which starts anywhere on the G-axis always moves toward higher $\mathfrak{H}$ until it finally approaches one of the three points P_-, P_+, or the origin—these are the only possible end points. If it enters either of the $\mathfrak{H} = 0$ loops (shaded) it will go to the corresponding maximum, either P_- or P_+; an eigensolution must therefore avoid the shaded area in order to reach the origin. The points P_-, P_+, and the origin represent constant solutions of the differential equations; by linearizing in the neighborhood of these constant solutions, it is easy to show that the representative point spirals into either P_- or P_+; on the other hand the origin is a saddle point.

With this qualitative information one may obtain the exact eigensolutions by the following numerical method. One finds by a numerical integration that one solution starting at $(G_0, 0)$ ends at P_+ and that another starting at $(G_1, 0)$ goes to P_-, and that neither curve goes below the G-axis. By narrowing the interval (G_0, G_1) one may then find the eigensolution to any desired accuracy; and if neither curve goes below the G-axis the corresponding eigensolution will be nodeless. By moving the starting point to the right one obtains eigensolutions with more nodes.

Thus the starting value of G may take on only a discrete set of values for given ν. (On the other hand, one may hold G_0 fixed and vary ν; then only particular values of ν will correspond to eigensolutions.) In the present problem ν is the mass of the pion and is experimentally fixed. In addition G_0 is fixed by the probability normalization in terms of g. Holding ν fixed, one varies G_0 (or g) until an eigenfunction is obtained. The eigenproblem thus establishes

a relation between g and ν. The procedure here is to assign to ν its experimental value and then to calculate g and other quantities of interest.

NORMALIZATION AND RESULTS

The following normalization condition was used:

$$\int\int \Psi^{+}(\gamma_4^{(1)} + \gamma_4^{(2)})\, \Psi d^3x\, d^3X = 1$$

which simplifies for the solution obtained to:

$$\int_0^{\infty} F(x)\, G(x)\, x^2\, dx = -\,|g|/64\pi.$$

With the parameter $\nu = 0.08$ the zero node solution was obtained with a differential analyzer. These solutions are plotted in Fig. 3 where $G(x)$ and $E(x)$ are shown. The probability density is shown in Fig. 4.

A phase plane analysis shows that for the "experimental" value of the parameter $\nu(=0.08)$ no eigensolutions exist for the interactions J_0, J_2, and J_3. We have no reliable results on J_4.

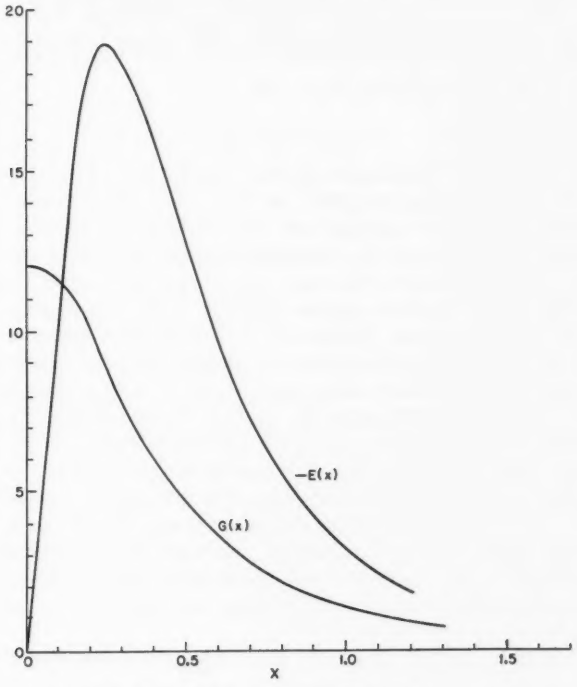

FIG. 3. Plot of $G(x)$, $E(x)$ as obtained on the differential analyzer.

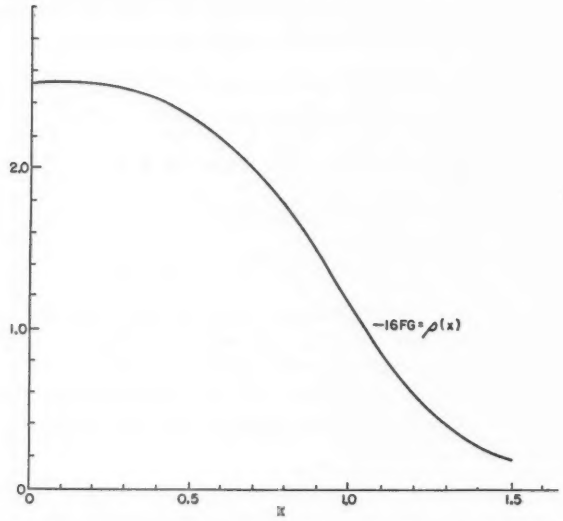

FIG. 4. Plot of $\rho(x) = -16F(x)\,G(x)$, using $G(x)$ from Fig. 3 and $F(x)$ calculated from eq. [31*c*].

Note: From the plot $\int -16\,F(x)\,G(x)\,x^2\,dx = 1.20$.

CONCLUSIONS

Although there is no theoretical justification for the physical model, still because of its mathematical simplicity we have used it to estimate the masses of the neutral and charged particles and their lifetimes for β and γ decay (9). (The initial wave function of the two-nucleon system is taken from the above calculation. The β-decay is a one-step process and the γ-decay involves two steps; the calculation therefore requires one lower order of perturbation theory than the conventional meson calculation. For example, γ-decay of the composite pion is pictured in just the same way as the γ-decay of positronium, and does not require a preliminary dissociation into a heavy particle pair.) The calculated mass difference between the neutral and the charged particles, as well as the lifetime for β-decay, is correct, but the γ-lifetime is 10^6 times too short. These results, however, depend mainly on the size of the localized wave function, not on its form, and hence tell nothing about details of the model.* To investigate these details one must reconsider the γ-lifetime, and one must also apply the same theory to the deuteron. As pointed out by Fermi and Yang the deep potential well in the pion must go over into a high repulsive barrier in the deuteron. That occurs only for certain choices of the interaction in the present model also.

As a result of its formal simplicity the fundamental equation [1] may be

**A discussion of the composite pion not employing a particular model has been given elsewhere (7). In equation (6) of that paper the inequality should be reversed, but the form, or even existence, of a universal Fermi interaction is still in doubt.*

looked at in several ways. Its interpretation in terms of a functional potential well has already been mentioned. Its similarity to some of the equations of current field theory may also be noted—including the nonlinearity; on the other hand it differs from these equations in not being an integral equation as well. Finally, it resembles especially the equations studied in Reference (8); in fact, it is the simplest nonlocal generalization of those equations.

The present investigation was intended to be primarily of methodological interest. It was successful in showing that equation [1] could be treated by the same phase space methods as were used earlier for the simpler equations described in Reference (8).

REFERENCES

1. BOHM, D. Phys. Rev. 84: 166. 1952.
2. DE BROGLIE, L. Une Nouvelle Théorie de la Lumière. Actualités scientifiques et industrielles. No. 181. Hermann & Cie., Paris. 1934.
3. DE BROGLIE, L. Compt. rend. 230: 1434. 1950.
4. DE BROGLIE, L. and TONNELAT, M. Compt. rend. 230: 1329. 1950.
5. EINSTEIN, A., PODOLSKY, B., and ROSEN, N. Phys. Rev. 47: 777. 1935.
6. FERMI, E. and YANG, C. N. Phys. Rev. 76: 1739. 1949.
7. FINKELSTEIN, R. Phys. Rev. 88: 555. 1952.
8. FINKELSTEIN, R., LELEVIER, R., and RUDERMAN, M. Phys. Rev. 83: 326. 1951.
9. GASIOROWICZ, S. G. Thesis, University of California at Los Angeles. 1952.
10. MOSELEY, H. M. and ROSEN, N. Phys. Rev. 80: 177. 1950.
11. ROSEN, N. Phys. Rev. 74: 128(A). 1948.
12. YANG, C. N. and TIOMNO, J. Phys. Rev. 79: 495. 1950.

CANADIAN JOURNAL OF PHYSICS

Notes to Contributors

Manuscripts

(i) ***General.*** Manuscripts should be typewritten, double spaced, on paper 8½×11 in. **The original and one copy are to be submitted.** Tables (each typed on a separate sheet) and captions for the figures should be placed at the end of the manuscript. Every sheet of the manuscript should be numbered.

Style, arrangement, spelling, and abbreviations should conform to the usage of this journal. Names of all simple compounds, rather than their formulas, should be used in the text. Greek letters or unusual signs should be written plainly or explained by marginal notes. Superscripts and subscripts must be legible and carefully placed.

Manuscripts should be carefully checked before they are submitted; authors will be charged for changes made in the proof that are considered excessive.

(ii) ***Abstract.*** An abstract of not more than about 200 words, indicating the scope of the work and the principal findings, is required, except in Notes.

(iii) ***References.*** References should be listed **alphabetically by authors' names,** numbered, and typed after the text. The form of the citations should be that used in this journal; in references to papers in periodicals, titles should not be given and only initial page numbers are required. All citations should be checked with the original articles and each one referred to in the text by the key number.

(iv) ***Tables.*** Tables should be numbered in roman numerals and each table referred to in the text. Titles should always be given but should be brief; column headings should be brief and descriptive matter in the tables confined to a minimum. Numerous small tables should be avoided.

Illustrations

(i) ***General.*** All figures (including each figure of the plates) should be numbered consecutively from 1 up, in arabic numerals, and each figure referred to in the text. The author's name, title of the paper, and figure number should be written in the lower left corner of the sheets on which the illustrations appear. Captions should not be written on the illustrations (see Manuscript (i)).

(ii) ***Line Drawings.*** Drawings should be carefully made with India ink on white drawing paper, blue tracing linen, or co-ordinate paper ruled in blue only; any co-ordinate lines that are to appear in the reproduction should be ruled in black ink. Paper ruled in green, yellow, or red should not be used unless it is desired to have all the co-ordinate lines show. All lines should be of sufficient thickness to reproduce well. Decimal points, periods, and stippled dots should be solid black circles large enough to be reduced if necessary. Letters and numerals should be neatly made, preferably with a stencil (**do NOT use typewriting**), and be of such size that the smallest lettering will be not less than 1 mm. high when reproduced in a cut 3 in. wide.

Many drawings are made too large; originals should not be more than 2 or 3 times the size of the desired reproduction. In large drawings or groups of drawings the ratio of height to width should conform to that of a journal page but the height should be adjusted to make allowance for the caption.

The original drawings and one set of clear copies (e.g. small photographs) are to be submitted.

(iii) ***Photographs.*** Prints should be made on glossy paper, with strong contrasts. They should be trimmed so that essential features only are shown and mounted carefully, with rubber cement, on white cardboard.

As many photographs as possible should be mounted together (with a **very** small space between each photo) to reduce the number of cuts required. Full use of the space available should be made and the ratio of height to width should correspond to that of a journal page; however, allowance must be made for the captions. Photographs or groups of photographs should not be more than 2 or 3 times the size of the desired reproduction.

Photographs are to be submitted in duplicate; if they are to be reproduced in groups one set should be mounted, the duplicate set unmounted.

Reprints

A total of 50 reprints of each paper, without covers, are supplied free. Additional reprints, with or without covers, may be purchased.

Charges for reprints are based on the number of printed pages, which may be calculated approximately by multiplying by 0.6 the number of manuscript pages (double-spaced typewritten sheets, 8½ × 11 in.) and making allowance for illustrations (not inserts). The cost per page is given on the reprint requisition which accompanies the galley.

Any reprints required in addition to those requested on the author's reprint requisition form must be ordered officially as soon as the paper has been accepted for publication.

Contents

Printed in Canada *by* University of Toronto Press